Aus dem Fachbereich Medizin

der Johann Wolfgang Goethe-Universität

Frankfurt am Main

Betreut an der

Dr. Senckenbergischen Anatomie

Institut Anatomie I

(Klinische Neuroanatomie)

Direktor: Prof. Dr. Thomas Deller

Functional changes in the dentate gyrus of wildtype and CAP23 transgenic mice following entorhinal denervation

Dissertation

zur Erlangung des Doktorgrades der Medizin

des Fachbereichs Medizin

der Johann Wolfgang Goethe-Universität

Frankfurt am Main

vorgelegt von

Mohammad Valeed Ahmed Sethi

aus Jeddah

Frankfurt am Main, 2018

Dekan:	Prof. Dr. Josef M. Pfeilschifter
Referent:	Prof. Dr. Thomas Deller
Korreferent:	Prof. Dr. Matthias Kieslich
Tag der mündlichen Prüfung:	28.02.2018

CONTENT

1 Zusammenfassung 10

2 Abstract 12

3 Introduction 13

3.1 Functional Anatomy of the Hippocampal Formation 13

3.1.1 The Hippocampus 14

3.1.2 The Dentate Gyrus 15

3.1.3 Extracellular FPs 17

3.1.4 The Dipole-Effect and the Hodgkin-Huxley-Model 20

3.2 Axonal Plasticity 20

3.2.1 Entorhinal Cortex Lesion / Entorhinal Denervation 21

3.2.2 GAP43 and CAP23/NAP22 22

4 Materials and Methods 26

4.1 Setup-Establishment 26

4.1.1 Anesthesia 26

4.1.2 Electrophysiological Stimulation and Recording 26

4.1.3 Placing the Stimulation Electrodes 27

4.1.4 Electrophysiological Measurements 29

4.1.5 Histological Control of Lesion Quality 30

4.2 Animals 30

4.3 Surgery and In-Vivo Electrophysiology 31

4.3.1 Anesthesia 31

4.3.2 Transection of the PP (ECL) 31

4.3.3 Electrophysiological Measurements 32

4.3.4 Perfusion and Immunohistochemistry 34

4.4 Data-Evaluation 35

4.4.1 Evaluation of the Electrophysiological Data 35
4.4.2 Latency-Shift Indicates Beginning of DG 35
4.4.3 Standardization of the Data 36
4.4.4 Current Source Density 36
4.5 Statistical Analysis 37
5 Results 38
5.1 Recording of Lamina-Specific Profiles Following Stimulation of the Contralateral Hilus or Entorhinal Cortex 38
5.1.1 CA1-Region 41
5.1.2 Dentate Gyrus 41
5.2 Shift of Onset Latency from CA1 to DG 42
5.2.1 Differences in Slope-Onset Latency in CA1 and DG 42
5.3 The Denervated DG Shows Shrinkage after ECL 47
5.4 In the Outer Molecular Layer There is an Enhanced Sink After Denervation in CAP23tg Mice 49
5.5 After Reinnervation of the OML the Granule-Cells Become More Excitable in CAP23tg Mice 51
6 Discussion 56
6.1 Electrophysiological Recordings of Layer-Specific Profiles in the Hippocampus and the Dentate Gyrus of Mice 57
6.1.1 Laminar Profile of the Hippocampus 57
6.1.2 Laminar Profile of the DG 58
6.2 The Latency-Shift as a Reliable Method to Identify the Hippocampal Fissure 59
6.2.1 Latency-Shift After Stimulation of the Contralateral Entorhinal Cortex 59
6.2.2 Latency-Shift After Stimulation of the Contralateral Hilar Mossy-Cells 62
6.2.3 Use of the Latency-Shift to Identify the Hippocampal Fissure 62

6.3 Degeneration-Induced Structural Changes in the Dentate Gyrus of Wildtype and CAP23tg Mice Following Entorhinal Cortex Lesion 63
6.3.1 Shrinkage of the ML in Wildtype and CAP23tg Mice 63
6.3.2 Control of the Lesion Quality with Acetylcholinesterase Staining 64
6.4 Axonal Sprouting and its Effects 64
6.4.1 Homotypic, Heterotypic, Homologue, and Heterologue Sprouting 64
6.4.2 Axonal Sprouting After ECL in WT Mice 65
6.4.3 Axonal Sprouting After ECL in CAP23tg Mice 66
6.5 Denervation-Induced Functional Changes 66
6.5.1 Functional Changes of WT Mice 66
6.5.2 Functional Changes of CAP23tg Mice 67
6.5.3 Comparison of WT and CAP23tg Mice 67
6.5.4 Restoration of Functionality 68
7 Clinical Implications and Conclusion 69
8 References 70
9 Curriculum Vitae 82
10 Danksagung 83
11 Schriftliche Erklärung 84

Figure 1: Sketch of sink-generation after stimulation of the performant path 19

Figure 2: Sketch of sink-generation after stimulation of the hilar mossy-cells 20

Figure 3: Schematic illustration of circuitry 27

Figure 4: Positioning of the electrodes in the DG.....28

Figure 5: Positioning of the electrode in the DG with corresponding evoked potentials 29

Figure 6: Overview of the animals used in this thesis 30

Figure 7: Setup for ECL.....32

Figure 8: Schematic illustration of places of stimulation.....33

Figure 9: Trace of recording electrode.....33

Figure 10: Control of electrode positioning 34

Figure 11: Example of a laminar profile with a corresponding histological profile after hilar stimulation (commissural fibers) 39

Figure 12: Example of a laminar profile (CSD-calculation) with a corresponding histological profile after hilar stimulation (commissural fibers) 40

Figure 13: Graph of mean FPs of the DG 42

Figure 14: Sample trace indicating the latency shift.....44

Figure 15: Mean response onset latencies for WT-mice without and with ECL.....45

Figure 16: Mean response onset latencies for CAP23tg-mice without and with ECL 45

Figure 17: Histological measurement of the depth of the hippocampal fissure 47

Figure 18: Hippocampus and DG of a CAP23tg mouse without and with ECL 48

Figure 19: Shrinkage of the ML after ECL 49

Figure 20: Graph of mean FPs of the DG of WT mice 50

Figure 21: Graph of mean FPs of the DG of CAP23tg mice 51

Figure 22: Average stimulus-induced FPs and calculated CSDs in the OML.....53

Figure 23: Average stimulus-induced FPs and calculated CSDs in the IML.....54

Figure 24: Average stimulus-induced FPs and calculated CSDs in the GCL 55

List of Abbreviations

AC	*Associational- and commissural pathway*
AChE	*Acetylcholin-Esterase*
CA1/3	*CA1/3-region (cornu ammonis)*
CAP23	*Cytoskeleton-associated protein 23*
CAP23tg	*CAP23-transgenic*
CSD	*Current source density*
DG	*Dentate gyrus*
EC	*Entorhinal cortex*
ECL	*Entorhinal cortex lesion*
EPSP	*Excitatory postsynaptic potential*
FP	*Field potential*
GABA	*Gamma-aminobutyric acid*
GAP	*Growth-associated protein*
GAP43	*Growth-associated protein 43*
GAP43tg	*GAP43-transgenic*
GC	*Granule-cell*
GCL	*Granule-cell layer*
IML	*Inner molecular layer*
IPSP	*Inhibitory postsynaptic potential*
MC	*Mossy-cell*
ML	*Molecular layer*
NAP22	*Neuronal tissue-enriched acidic protein 22*
NCAM	*Neuronal cell adhesion molecules*
OML	*Outer molecular layer*
PHAL	*Phaseolus-vulgaris leukagglutinin*
PP	*Perforant path*
SC	*Schaffer collateral*

SEM	*Standard error of the mean*
WT	*Wild-type*

1 ZUSAMMENFASSUNG

Nach entorhinaler Deafferenzierung des Gyrus Dentatus der Hippokampusformation kommt es innerhalb von wenigen Wochen zur partiellen Reinnervation der deafferenzierten Neurone durch Kollateralsprossung überlebender Axone. Bislang ist noch unbekannt, welchen funktionellen Einfluss diese Reinnervation auf das Gesamtnetzwerk des Gyrus Dentatus hat.

Zur Klärung dieser Frage haben wir den Einfluss der axonalen Sprossung auf die Aktivität des neuronalen Netzwerkes im Gyrus Dentatus untersucht. Hierzu wurden zum Einen Wildtyp-Mäuse (WT Mäuse), die ein normales Sprossungsverhalten nach Läsion aufweisen, und zum Anderen CAP23-überexprimierende (CAP23tg) Mäuse, die über eine verstärkte axonale Wachstumsfähigkeit verfügen und verstärkte Sprossung zeigen, elektrophysiologisch analysiert und miteinander verglichen.

Im Rahmen der Experimente wurden zunächst die entorhinalen Fasern zum Gyrus Dentatus in WT Mäusen und CAP23tg Mäusen stereotaktisch durchtrennt. Anschließend überlebten die Mäuse für 4-6 Wochen und wurden - nach partieller Reinnervation des Gyrus Dentatus durch die sprossenden Axone - elektrophysiologisch untersucht (extrazelluläre Ableitungen im Gyrus Dentatus zur Messung evozierter Potentiale). Als Vergleichsgruppen dienten gleichaltrige Mäuse ohne Läsion. Die Axonsprossung und die Positionierung der Elektroden wurden histologisch überprüft.

Bei den elektrophysiologischen Untersuchungen wurden laminäre Profile bestimmt und eine "current-source-density" Analyse durchgeführt. In den läsionierten CAP23tg Mäusen zeigte sich im Vergleich zu den läsionierten WT Mäusen eine deutliche Verstärkung des "current-sink" in der deafferenzierten äußeren Molekularschicht des Gyrus Dentatus sowie eine Verstärkung der Exzitation im Bereich der Körnerzellschicht.

Diese Befunde legen nahe, dass die verstärkte Sprossung von überlebenden Axonen zu einer verstärkten Exzitation der Körnerzellen führt. Insofern könnte eine Verstärkung der Axonsprossung zwar einerseits zu einer schnelleren Reinnervation der Körnerzellen führen, andererseits aber auch die Exzitabilität der Körnerzellen

erhöhen und auf diese Weise eine posttraumatische Übererregbarkeit des neuronalen Gewebes begünstigen. Diese beiden Effekte wären bei therapeutischen Strategien zur Verstärkung der Sprossung nach einer Läsion gegeneinander abzuwägen.

2 ABSTRACT

After entorhinal deafferentiation of the hippocampal dentate gyrus a reinnervation of the denervated neurons by axon collaterals can be observed. This process takes place in a matter of weeks. However, the overall functional effect on the hippocampal network is still unclear.

In an effort to investigate this effect of axonal sprouting on the neuronal network of the dentate gyrus we compared the electrophysiological response of the dentate gyrus after electric stimulation in wild-type mice (WT mice) with a normal post-lesion sprouting, with genetically modified mice with an overexpression of the growth-protein CAP23 (cytoskeleton-associated protein 23). CAP23 overexpressing mice (CAP23tg mice) are known to have an enhanced axonal growth and sprouting after lesion.

The mice (both the WT as well as the CAP23tg mice) were deeply anesthetized and a lesion of the perforant path was induced stereotactically with a wire knife. After that the mice were permitted to survive for 4-6 weeks for partial reinnervation of the dentate gyrus before they were again operated and evoked potentials were measured (extracellular recordings of evoked potentials in the dentate gyrus). Non-lesioned litter-mate mice were taken as reference. The sprouting and the correct position of the electrodes was confirmed histologically.

For electrophysiological investigation we assessed laminar profiles and calculated a current-source density (CSD). In lesioned CAP23tg mice compared to lesioned WT mice this CSD-analysis revealed a significant enhancement of the current sink in the area of deafferentiation (outer molecular layer) and a significant excitation in the granule-cell layer.

Our results show that axonal sprouting seems to enhance the excitability of granule-cells. Thus, even if an enhanced axonal sprouting might accelerate the reinnervation of denervated dendrites after lesion, but it also leads to posttraumatic hyperexcitability of the neuronal network. In a therapeutic approach of fascilitating axonal sprouting this hyperexcitability has to be taken into consideration.

3 INTRODUCTION

The hippocampal formation has fascinated scientists attention since the first dissections took place back in Classical Egypt (Andersen et al., 2007). Located in the medial temporal lobe it contains millions of neurons organized in a strict laminar pattern forming a unique network (Golgi et al., 2001). In modern times this laminar pattern has made the hippocampus a model region to study basic functions of neurons and small networks (Deller, 1998).

3.1 FUNCTIONAL ANATOMY OF THE HIPPOCAMPAL FORMATION

Since Lorente de Nó offered the first theoretical explanation for the generation of extracellular field potentials (FP) in 1947 (Lorente de Nó, 1947), many scientists have used the hippocampal formation for the analysis of FPs due to “the dense packing of the cell bodies, the roughly parallel position of the apical dendrites of hippocampal neurons, and the ease with which they can be synchronously activated” (Andersen et al., 2007). Subsequently the hippocampus has been subject to many research efforts especially to investigate electrophysiological network properties in functions such as memory or emotions (Papez, 1995; Scoville and Milner, 1957).

Unlike the common organizational feature of reciprocal connections in the neocortex excitatory interconnections of the hippocampal formation are largely unidirectional (Andersen et al., 2007; Ramón and Cajal, 1893). For a better overview the main path of excitation should be kept in mind. The main excitatory input to the hippocampal formation is via the entorhinal cortex (EC). The EC delivers excitation via the perforant path (PP) mainly to the dendritic layer of the dentate gyrus (DG). The granule-cells (GC) of the DG project to CA3-region (CA3) via mossy fibers. CA3 activates CA1-region (CA1) via the Schaffer collaterals (SC). CA1 sends axons back to the EC either directly or via the subiculum (Amaral and Witter, 1989). Other excitatory pathways are also present and will be introduced separately.

3.1.1 The Hippocampus

The hippocampus was first described by Julius Caesar Arantius in 1587 (Arantius, 1587) and is named after the similar looking animal. The major part of the hippocampus is the cornu ammonis (CA) named after the mythological Egyptian god Amun Kneph, whose symbol was a ram. It consists of two major regions, CA1 and CA3, while CA2 is a linking part (Andersen et al., 2007).

3.1.1.1 THE PYRAMIDAL CELLS

The pyramidal cells are the principal cells of the hippocampus. They are located in *stratum pyramidale*, the cell-layer of the hippocampal region. This pyramidal cell layer is surrounded by *stratum oriens*, which is the basal dendritic layer and *stratum radiatum*, which is the proximal apical dendritic layer. The dendritic arbor reaches the hippocampal fissure where it forms the *stratum lacunosum-moleculare* together with afferent fibers from the EC (Andersen et al., 2007; Andersen et al., 1971).

3.1.1.2 EXCITATORY AND INHIBITORY INPUT TO THE CA1-REGION

CA1 has three dendritic layers, namely *stratum oriens*, *stratum radiatum* and *stratum lacunosum-moleculare*. In earlier studies Buzsáki demonstrated that the main input to *stratum oriens* originates from CA1-region-SCs, while *stratum radiatum* receives input from CA3-region-SCs making the *stratum radiatum* the main entry point for excitation via the hippocampal circuit (Buzsáki and Eidelberg, 1982). The information flow arrives via the mossy fibers of the GCs, reaches the CA3-pyramidal cells, which in turn activate CA1-pyramidal cells of both hemispheres via SCs. Excitation of the pyramidal cells however, also arises from the EC via *stratum lacunosum-moleculare* (Blackstad, 1958; Megias et al., 2001; Blackstad, 1958). The EC also has a projection to the contralateral CA1-region via the temporo-ammonic pathway (Yang et al., 2006). But the overall impact of the EC on the pyramidal cells is weak, and the main excitation is delivered by SCS as they innervate the spiny *stratum radiatum* and *oriens* instead of the much more inhibited and distal *stratum lacunosum-moleculare*, where synapses are formed mainly on the shaft and not on the much more excitable spines (Blackstad, 1958; Megias et al., 2001).

In addition to the excitatory network after activating the CA1-region, there is a relevant regulatory inhibitory network, mainly based on interneurons. Amongst others the *oriens-alveus/lacunosum-moleculare* (O-LM) interneurons project to the *stratum lacunosum-moleculare*, thus regulating the excitability of the pyramidal cells for excitation originating from the EC. The O-LM, as well as all the other inhibitory influences in the CA1-region, use gamma-aminobutyric acid (GABA) as the principal neurotransmitter (Andersen et al., 2007; Ribak et al., 1986; Nadler et al., 1974).

3.1.2 The Dentate Gyrus

The V-shaped DG comprises the *fascia dentata*, which encloses a cell-region called the polymorphic cell layer, also referred to as the “hilus”. The *fascia dentata* consists of the granule-cell layer (GCL) which is next to the hilus, and the molecular layer (ML), reaching the outer edge of the DG at the hippocampal fissure (Andersen et al., 2007). While the polymorphic cell layer and the GCL contain numerous different neurons, the ML is formed by the dendritic arbor of the GCs, afferent fibers and a small number of GABAergic inhibitory interneurons (Ceranik et al., 1997). The ML itself is divided into three parts, the inner molecular layer (IML), next to the GCL, the middle molecular layer (MML), and the outer molecular layer (OML) (Gall et al., 1980). This division is based on the different fibers which terminate in the three zones. In this thesis, however, we refer to the MML plus the OML as “OML”, which appears to be legitimate because both the layers receive excitatory input from the pyramidal cells of layer II of the EC (Schwartz and Coleman, 1981).

3.1.2.1 DENTATE GRANULE-CELL

The main cells of the DG are the granule-cells. They are densely packed with few glial cells in between. GCs have a characteristic cone-shaped tree of spiny dendrites, with its branches directed towards the hippocampal fissure. Usually the dendritic arbor of the suprapyramidal GCs tends to be larger than the one of the GCs of the infrapyramidal blade (Andersen et al., 2007).

Uncommon for brain structures, proliferation and neurogenesis persist in the DG into adulthood and appear to be under environmental control (Rapp and Gallagher, 1996). Nevertheless, except for infant and juvenile mice who can increase the number of GCs

in socially complex i.e. “enriched” environments (Kempermann et al., 1997), the total number of GCs in adulthood does not vary (Rapp and Gallagher, 1996). With specific stimulation paradigms proliferation and survival of newly generated neurons can occur in adult animals as well but without a significant impact on the volume of the DG or the total number of GCs (Kempermann et al., 1998).

The GCs are the only actual “principal” cells of the DG, hence they are the only cells sending axons out of the DG to other structures of the hippocampal formation e.g. the CA3-region. Beside them the mossy-cells (MC) also send axons out of the DG, but only in order to innervate the contralateral DG, thus staying within the dentate region (Prang et al., 2003).

3.1.2.2 MOSSY-CELLS

The MCs present the most prominent cell-type of the hilus. They are located underneath the GCL, forming a dendritic arbor within the hilus (Scharfman and Schwartzkroin, 1988). It is mainly the mossy fibers of the GCs which reach the dendritic arbor. However, also CA3-pyramidal cells send axon collaterals back into the hilus and innervate the MCs (Scharfman, 2007). MCs themselves have an excitatory influence on the GCs as they reach the dendritic arbor of the GCs at the IML of both hemispheres (Andersen et al., 2007; Prang et al., 2003). However, MCs also have an inhibitory input to the GCs via GABA-positive synapses, thus playing a pivotal role in the generation of epilepsy (Sloviter, 1994a).

3.1.2.3 EXCITATORY AND INHIBITORY AFFERENTS TO THE DG

The main excitatory input to the DG arises from the EC and terminates in the OML (Sloviter, 1994b). For a long time the concept that the OML is exclusively the termination zone for afferents originating from the EC was prevalent, before it could be shown that also GABAergic hilar interneurons send commissural axons to the OML (Deller et al., 1995b). This inhibitory input may play a role in the regulation of the DG excitation, as disinhibition of the DG facilitates seizures (Kobayashi and Buckmaster, 2003).

The MCs also have a net excitatory effect on the GCs of both hemispheres as they stimulate dendrites in the IML via the associational- and commissural (AC) pathway.

The GC-dendrites in the IML have fewer dendritic spines in comparison to the dendritic branches in the OML. Thus, it has been suggested that the main excitatory input to the DG comes from afferents terminating in the OML (Claiborne et al., 1990; Desmond and Levy, 1982, 1985).

3.1.3 Extracellular FPs

Recordings of extracellular FPs are based on the concept of differences in potentials at semi-permeable membranes, such as the cell membrane. This potential difference is based on the electrostatic and the osmotic interactions of ions along cell membranes (Goldman, 1943). If, for example, a cell membrane is permeable for sodium ions, it tends towards establishing an osmotic equilibrium at the cost of an electrostatic charge. This is done until the force for establishing an osmotic equilibrium and the opposing force deriving from the electrostatic potential differences are equal. Thus the osmotically driven electrostatic potential difference leads to the membrane potential. This correlation is mathematically described by the Goldman-Hodgkin-Katz voltage equation, which itself is derived from the Nernst equation. However, the Goldman-Hodgkin-Katz voltage equation takes into account all ions for which cell membranes are generally permeable (Goldman, 1943). The equation is as follows for sodium-, potassium- and chloride-ions:

$$E(Na^+, K^+, Cl^-) = 61.5\,mV\ \log\left(\frac{[Na^+](outside) + [K^+](outside) + [Cl^-](inside)}{[Na^+](inside) + [K^+](inside) + [Cl^-](outside)}\right)$$

In order to further understand the neurophysiological processes, one has to bear in mind the different ion concentrations in- and outside of the neurons. While sodium and chloride have a much higher concentration outside of the neurons, they thus have a tendency to move into the cells, potassium has a higher concentration inside of the neurons and has a reciprocal tendency. This concentration gradient is generated by the sodium-potassium ATPase (Lees, 1991).

3.1.3.1 GENERATION OF SINK AND SOURCE

The above mentioned electrochemical gradient describes the membrane potential of a cell. In case of excitation however, a depolarization occurs, while in case of inhibition a hyperpolarization opposes the excitation. There are different mechanisms leading to

de- or hyperpolarization. They have in common, however, that depolarization is mainly an influx of sodium ions, while a hyperpolarization can be caused by an outflow of potassium ions or an influx of chloride ions. The depolarization plays a pivotal role for generating an action potential, thus activating the function of the cell (Hodgkin and Huxley, 1952) (see also 3.1.4).

In order to understand the physiological processes and the distribution of current sink and current source, the GC can serve as a model:

3.1.3.2 STIMULATION VIA THE ENTORHINAL CORTEX

The excitatory EC stimulation leads to an activation of NMDA-glutamate-receptors, thus leading to a sodium influx in the OML. This influx of sodium is due to its gradient. As the concentration of sodium outside the cell is much higher than inside it, opening up a passive sodium channel like the NMDA-receptor leads to a strong influx of sodium-ions. This again leads to a loss of protons outside the dendrites at the site of the influx. For some time there is a misdistribution of positive and negative ions outside the cell which generates an electric charge. As there is a negativity just outside the cell at the site of the influx there is considered to be a sink (sodium-ions sinking into the cell). As a logical consequence of the sink at the OML there has to be a relative positivity somewhere else. Considering the fact that the hippocampal fissure just superficial of the OML has a very poor electric conductivity compared to the dendritic layers surrounding it (Holsheimer, 1987) and bearing in mind the electrostatic shift of electric charge the source has to be in the IML and the GCL (Figure 1).

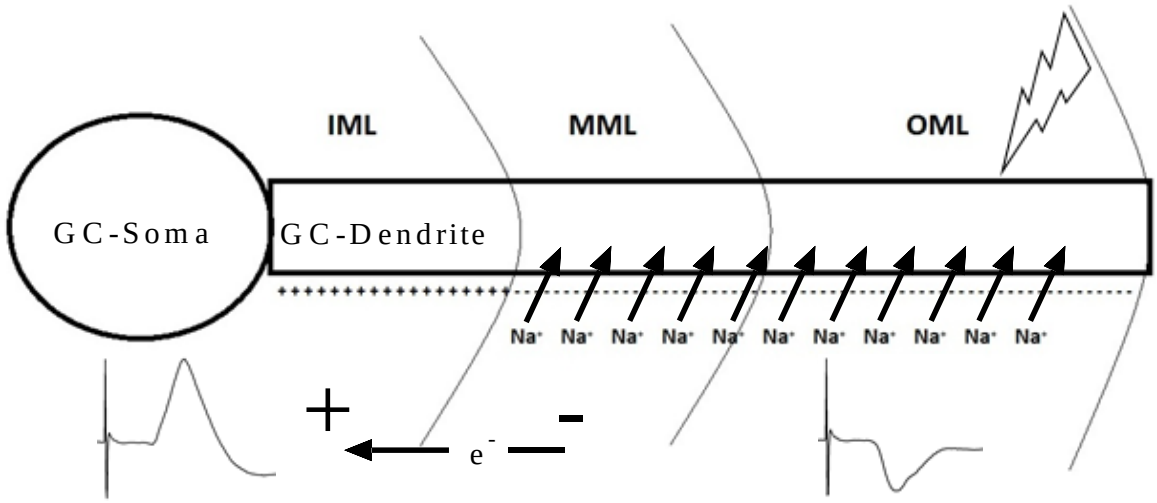

Figure 1: Sketch of sink-generation after stimulation of the performant path
This sketch shows the generation of the sink in the OML/MML (Excitation by PP). Due to the influx of sodium-ions the negative charge outside the cell rises, which can be seen in the negative FP if recorded from the OML/MML. Meanwhile the IML has a positive FP, though not clearly distinguishable from the much stronger source of the soma.

3.1.3.3 STIMULATION VIA THE MOSSY-CELLS

The stimulation of the MCs leads to an activation of the GCs via the IML. One can also say that this actually is the definition of the IML, being innervated by the MCs. The innervation is glutamatergic, thus is excitatory (Andersen et al., 2007). This excitation leads again to a sodium influx and generates a sink in the IML (Figure 2).

Now when it comes down to an activation meaning there is a sink, then the dipole effect applies, which will be discussed shortly. Activation of IML leads to a source in the OML and the GCL. The OML-source is surrounded by the sink of the *stratum radiatum* and *stratum lacunosum-moleculare* of the hippocampus and the sink in the IML, thus is clearly visible in manner of electrophysiological measurements. So if one is recording in the OML a slight source-response is measurable in the CSD. Meanwhile the IML has a clear sink-signal (Clusmann et al., 1994).

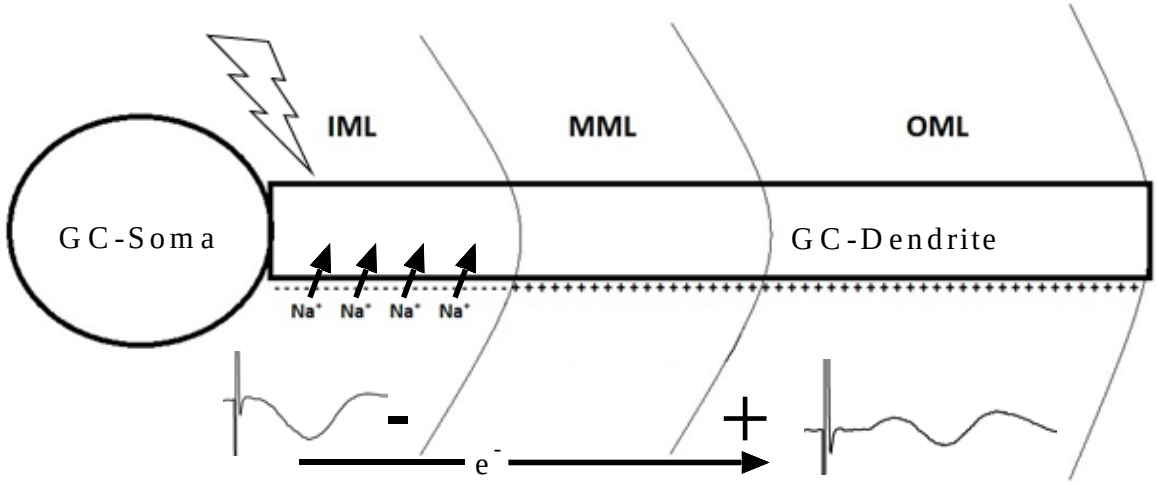

Figure 2: Sketch of sink-generation after stimulation of the hilar mossy-cells
This sketch shows the generation of a sink at the IML (excitation by mossy-cell axons). Due to the influx of sodium-ions at the IML, there is a higher negative charge outside.

3.1.4 The Dipole-Effect and the Hodgkin-Huxley-Model

The above mentioned phenomenon is described by the Hodgkin-Huxley-Model (Hodgkin and Huxley, 1952). If an electric charge is created like on the dendrite of the neuron, then there is a dipole moment, which is dependent on the charge and the distance. If there is an influx of positively charged sodium ions like in our experiments, then this will leave a negativity at the site of the influx on the outside of the cell and a positivity inside the cell. This positivity then induces a dipole moment, which leads to an electrostatic attraction of electrons to the site of the influx of sodium. The electrons inside the dendrites come from those parts of the dendrite, where there is no influx. In turn, this shift of electrons towards the site of activation leaves behind a positivity. In this context the electric resistance in- and outside the cell plays an important role for creating the potential difference. These phenomena appear almost instantaneously so that a negative voltage can be measured at the location of the “sink” and a positive voltage at the “source”.

3.2 AXONAL PLASTICITY

The term “axonal plasticity” subsumes axonal reactions to changes in network activity, injury, insult, or degeneration of the central nervous system and, at the structural level,

includes modifications of axonal length, branching, and connections (Andersen et al., 2007). A major obstacle for axonal regeneration in the injured CNS is the gliotic scar which is formed by proliferating astrocytes and connective tissue cells, which can hardly be penetrated by regenerating or sprouting axons (Perederiy and Westbrook, 2013; Sofroniew and Vinters, 2010; Bovolenta et al., 1991).

In this context the hippocampal formation plays an exceptional role, as the connections between the hippocampal formation and the septum were used to demonstrate axonal sprouting by Raisman back in 1969 (Raisman, 1969). Raisman was also able to show that sprouting axons can re-occupy vacated postsynaptic sites after lesion. In a later study Raisman and Field were even able to show an axonal sprouting to the contralateral hemisphere (Raisman and Field, 1973). In this study a unilateral fimbrial lesion was performed giving rise to a significant sprouting of the contralateral fiber system. One year later Steward found the same phenomenon after entorhinal cortex lesion (ECL) and axonal sprouting from the contralateral EC via the temporodentate pathway in the rat (Steward et al., 1974). Nevertheless, according to the current state of knowledge this projection does not exist in the mouse. Yet, with the ECL, a unique model of post-injury plasticity was introduced.

3.2.1 Entorhinal Cortex Lesion / Entorhinal Denervation

The ECL model is a classical model to study the postlesional plasticity in the adult brain (Deller et al., 2007; Deller and Frotscher, 1997). By lesioning the EC or by transecting the PP the major excitatory afferents to the DD and hippocampus are lost (Knowles, 1992; Perederiy and Westbrook, 2013). The ECL has advantages over other lesion models since the site of the lesion is far away from the site of denervation, in our experiments the site of analysis. Thus, the area of the injury with its injury-induced changes does not directly affect the reorganizational processes of the DG (Perederiy and Westbrook, 2013). Furthermore, the strict laminar pattern of the hippocampus and the DG with specific termination areas for each input facilitates investigations (Hjorth-Simonsen and Jeune, 1972; Perederiy and Westbrook, 2013).

As described above, the EC terminates in the outer two thirds of the ML where its axons form 80-90% of all synapses. The remaining axons can sprout after ECL and

can innervate the vacated synaptic sites. Depending on the fiber system that sprouts, this axonal sprouting can be homotypic (glutamatergic axonal sprouting) e.g. MC axons, or heterotypic (e.g. cholinergic axonal sprouting) (Perederiy and Westbrook, 2013). The latter one comes along with an increase in the concentration of acetylcholine-esterase (AChE), which is commonly accepted as a histochemical marker for the extent and quality of an ECL (Vuksic et al., 2011). Certain morphological changes of the dendrites however occur following the loss of the main excitatory input to the DG including the retraction of dendrites leading to a less complex dendritic arbor, the loss of dendritic segments, and the reduction of dendritic spines (Vuksic et al., 2011; Perederiy and Westbrook, 2013).

These changes come along with morphological changes of the glia. There is evidence that the glial scar is not only formed in the area of the injury, but also as a result of degenerating synapses, which has been shown in former studies in experiments following mossy fiber lesion and showing most pronounced proliferation of microglial cells after 3 weeks (Finsen et al., 1993) and also in the case of Alzheimer's disease and non-Alzheimer type frontal lobe degeneration (Brun et al., 1995). However, Repressa stated that there was no proliferation of glial cells within fields with exclusive axon-terminal degeneration, such as the ML of the DG, but rather a hypertrophy of astrocytes (Repressa et al., 1995). He further assumed that astrocytes as well as other glial cells may play a pivotal role for axonal outgrowth by secretion and expression of signaling molecules such as neural cell adhesion molecules (NCAM) or tenascin (Repressa et al., 1995). Hence axonal reorganization in the molecular layer is facilitated by glial cells making the ECL an even more practical model to investigate on postlesional plasticity. However, axonal outgrowth stimulated by NCAM requires growth-associated proteins such as growth-associated protein 43 (GAP43) and CAP23/NAP22. It is known that these proteins are expressed in growing axons (Meiri et al., 1986).

3.2.2 GAP43 and CAP23/NAP22

Considering the vast amount of synaptic connections in the nervous system a strict control of axonal outgrowth is mandatory. In this context several extrinsic and intrinsic determinants have been identified so far, regulating the process of axonal sprouting.

Extrinsic determinants are signaling molecules found in the local environment which stimulate, attract, repel or inhibit axonal sprouting by multiple mechanisms. Furthermore, these extrinsic determinants may in some cases also regulate the expression of intrinsic determinants (Caroni, 1997).

A group of molecules which are considered “intrinsic determinants of axonal growth” are the so called “growth-associated proteins” (GAPs). These GAPs show an increased expression during axonal growth or regeneration over long distances in axonal growth cones (Morita and Miyata, 2013). In mice axonal growth mainly correlates with the GAP43 and the 22kDa neuronal tissue-enriched acidic protein (NAP22). The 23kDA cytoskeleton-associated protein (CAP23) can be found in the chicken and is the chicken homologue of NAP22. These proteins are GAPs and regulate axonal growth and axonal sprouting (Caroni, 1997; Voelcker, 2012). For experimental purposes a CAP23 transgenic mouse has been generated which expresses the chicken-homologue CAP23 as a transgene in addition to the endogenous mouse NAP22. This makes it possible to identify the genes encoding for the two homologue proteins in the same animals (Voelcker, 2012).

3.2.2.1 GAP43

GAP43, also known as neuromodulin, B-50, P-57, F1, and pp46 (Denny, 2006), is a neuron-specific phosphoprotein that plays an important role in synaptic plasticity during development but also in the adult (Aigner et al., 1995; Gorgels et al., 1989; Morita and Miyata, 2013).

During development synthesis and axonal transport of GAP43 persist throughout axogenesis and synaptogenesis, before declining significantly subsequent to the establishment of stable synaptic connections. The levels of GAP43 are highest during the first three postnatal weeks before rapidly decreasing (Morita and Miyata, 2013). However, GAP43 activity remains high in *stratum lacunosum-moleculare* of CA1 and in the IML of the DG. In neurons the highest expression levels of GAP43 are observed in the growth cones of sprouting axons (Benowitz et al., 1988). The expression of GAP43 is also elevated in injured neurons after nerve injury. Van der Zee was able to show a significantly elevated GAP43 mRNA expression in the cell-bodies of the sciatic nerve in the dorsal root ganglia of up to 10 times the basal level of GAP43 mRNA two

days after crushing the peripheral nerve, with a significant rise of GAP43 protein after 40 hours already (Van der Zee et al., 1989).

Overexpression of GAP43 leads to an enhanced ability for axonal sprouting (Frey et al., 2000). Bomze et al. were able to show that overexpression may elicit long axon extension by adult dorsal root ganglion neurons in-vitro (Bomze et al., 2001). On the other hand GAP43 knock-out mice show a higher rate of postnatal mortality combined with wiring abnormalities resulting in disrupted cortical maps (Maier et al., 1999; Voelcker, 2012).

GAP43 mainly causes filopodial extension at the growth cone, thus facilitating spreading, branching and adhesion of the growing axon (Benowitz and Routtenberg, 1997). Its function is associated with proteins of the Ras superfamily of small GTPases like Rab, Ra1A, Ra1B, and proteins belonging to the Rho GTPase family like RhoA, Rac1, and cdc42 (Denny, 2006).

3.2.2.2 CAP23/NAP22

CAP23/NAP22 is a brain-specific protein characterized first in chicken brain as a 23 kDa cortical cytoskeleton-associated protein (Widmer and Caroni, 1990). Later a 22 kDa neuron-specific acidic protein as its homologue was discovered in the rat (Maekawa et al., 1993). CAP23/NAP22 is a prominent substrate of protein kinase C with calmodulin as a regulator of phosphorylation (Matsubara et al., 2004).

Like GAP43 it is strongly expressed during development, it remains in some brain structures throughout adulthood and may be upregulated during nerve regeneration (Frey et al., 2000). Overexpression of CAP23/NAP22 also enhances nerve growth and sprouting. Thus, CAP23/NAP22 and GAP43 are closely related functionally. In an experimental approach Frey was able to show that while CAP23/NAP22 knockout mice exhibited an increased rate of postnatal mortality, not more than 10% survived up to adulthood, weighed 50% less than their wild-type littermates, and had broader ventricles. CAP23/NAP22 knockout mice with a knockin of GAP43 into the CAP23 locus showed a normal survival with almost no structural and functional abnormalities (Frey et al., 2000).

Like GAP43, CAP23/NAP22 also causes filopodial extension at the growth cone, thus facilitating spreading, branching and adhesion of growing axon. The molecular mechanisms of both proteins are comparable (Voelcker, 2012).

3.2.2.3 CAP23/NAP22 IN MOSSY-CELLS

CAP23/NAP22 show a distribution similar to the one of GAP43 with a high concentration mainly in axon terminals and synapses. In the hippocampal formation the protein was found in a high concentration mainly in mossy fibers of the GCs as well as in the dendritic layers of CA1, CA2, CA3 and GCL. Immunohistochemically there was no evidence for CAP23/NAP22 in any cell bodies of the hippocampal formation. This supports its correlation with axonal and synaptic plasticity (Iino et al., 1999). In our study CAP23/NAP22 activity in MCs is crucial, as after ECL sprouting of MC axons can be observed in the mouse. In a preliminary report it has been shown in transgenic mice overexpressing GAPs that the strength and extent of this translaminar commissural sprouting depends strongly on the intrinsic growth competence of MCs deriving from GAPs (Del Turco et al., 2003).

Species	**Mus musculus**	**Gallus gallus**	**Mus musculus**
Name of gene	Basp1 Synonyme: NAP22	Basp1 Synonyme: CAP23	Basp2 Synonyme: GAP43
Name of protein	Brain acid soluble protein 1; 22 kDa neuronal tissue-enriched acidic protein Abbreviation: NAP22	Brain acid soluble protein 1 homologue; 23 kDa cortical cytoskeleton associated protein Abbreviation: CAP23	Brain acid soluble protein 2; Growth-associated protein; Neuromodulin Abbreviation: GAP43
Accession Number	Q91XV3	P23614	P06837

Table 1: Names of genes and corresponding proteins
This table characterizes the genes and the corresponding proteins used in this study. This table is a modified and translated version of a table used in the MD-thesis of Voelcker (Voelcker, 2012).

4 MATERIALS AND METHODS

4.1 SETUP-ESTABLISHMENT

Before the relevant experiments could be performed, a setup was established for simultaneous stimulation of the hippocampal formation from the contralateral hilus, as well as the contralateral EC.

4.1.1 Anesthesia

All surgeries were performed under deep anesthesia: meditomidin (0.5µg/g body weight (bw)), midazolam (5µg/g bw), and fentanyl (0,05µg/g bw) injected intraperitoneally. Anesthesia was upheld by injecting 2µg Medetomidin, 20µg Midazolam and 0.2µg Fentanyl every 2 hours intraperitoneally. Animals were monitored for responses to pain stimuli, and surgery was performed when animals failed to respond. Local anesthesia (Scandicain, 0.05ml of 1% solution) was also applied onto the skull and into the overlying skin to minimize pain. Body temperature was continuously monitored using a TCAT-2LV Controller (Physitemp Instruments, Clifton, New Jersey, USA). All experiments were carried out in accordance with German laws governing the use of laboratory animals.

4.1.2 Electrophysiological Stimulation and Recording

Biphasic stimulation of 800µA of current intensity for 0.1s was generated by a STG 1002 (a 2-channel-stimulation unit) with an integrated stimulus isolation unit (Multi Channel Systems, Reutlingen, Germany) and applied via stimulation electrodes. For PP stimulation a concentric bipolar electrode with 0.5mm distance between tip and shaft (NE-100, 0.5mm tip separation; Rhodes Medical, Summerland, CA, USA) was used while for commissural stimulation a concentric bipolar electrode with 0.25mm distance between tip and shaft (SNE-100, 0.25mm tip separation; Rhodes Medical, Summerland, CA, USA) was utilized. Both stimulations were applied on the right hemisphere. Recordings were made on the left hemisphere with a glass-electrode filled with 0.9% sodium-chloride solution and attached with a silver wire. Potentials were amplified by a Grass P55 A.C. preamplifier (Astro-Med, Rodgau, Germany), digitalized

by Digidata 1440A (Molecular Devices, Ismaning, Germany) and displayed on pClamp 9.0 computer system Clampex (Axon instruments, Union City, CA, USA). A schematic of this circuitry can be seen in Figure 3.

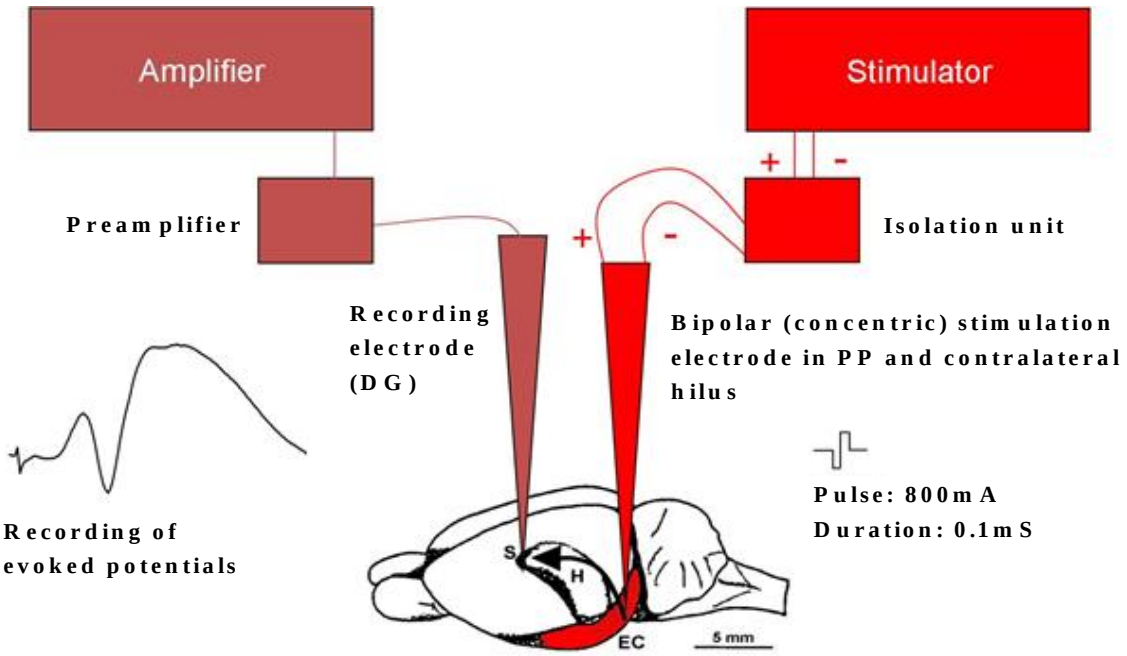

Figure 3: Schematic illustration of circuitry
This figure shows a schematic illustration of the circuitry used for stimulation and recording as described by Jedlicka, Schwarzacher and colleagues (Jedlicka et al., 2009). The picture shows the circuitry used for an ipsilateral PP stimulation of the DG on the left hemisphere.

4.1.3 Placing the Stimulation Electrodes

In order to place the stimulation electrodes, mice were fixed in a stereotactic head holder. The position of electrodes was chosen using a mouse brain atlas (Franklin and Paxinos, 1997) and on the basis of previous studies of ipsilateral PP stimulation in the mouse in vivo (Namgung et al., 1995). For positioning of the electrodes small holes were drilled through the skull. Both stimulation electrodes were placed into the right hemisphere. The electrode for PP stimulation (see also 4.1.2) was positioned in the angular bundle of the medial PP (4.0mm posterior and 2.0 – 2.5mm lateral to bregma). The electrode for hilar stimulation (see also 4.1.2) was placed in the hilus of the DG (2.0mm posterior and 1.2mm lateral to bregma). Placement of the electrodes required several steps which had to be performed in sequence. This resulted in an optimal placement of the electrodes in the PP and the hilus. First, the position of the stimulating

electrode in the PP was optimized. For this the electrode for PP stimulation was preliminarily placed into the PP while the electrode for the hilar stimulation was inserted into the DG. In this initial setting the electrode in the DG was used to detect the stimuli generated by the stimulation electrode in the PP. The strength of the recording was used to position the PP electrode.

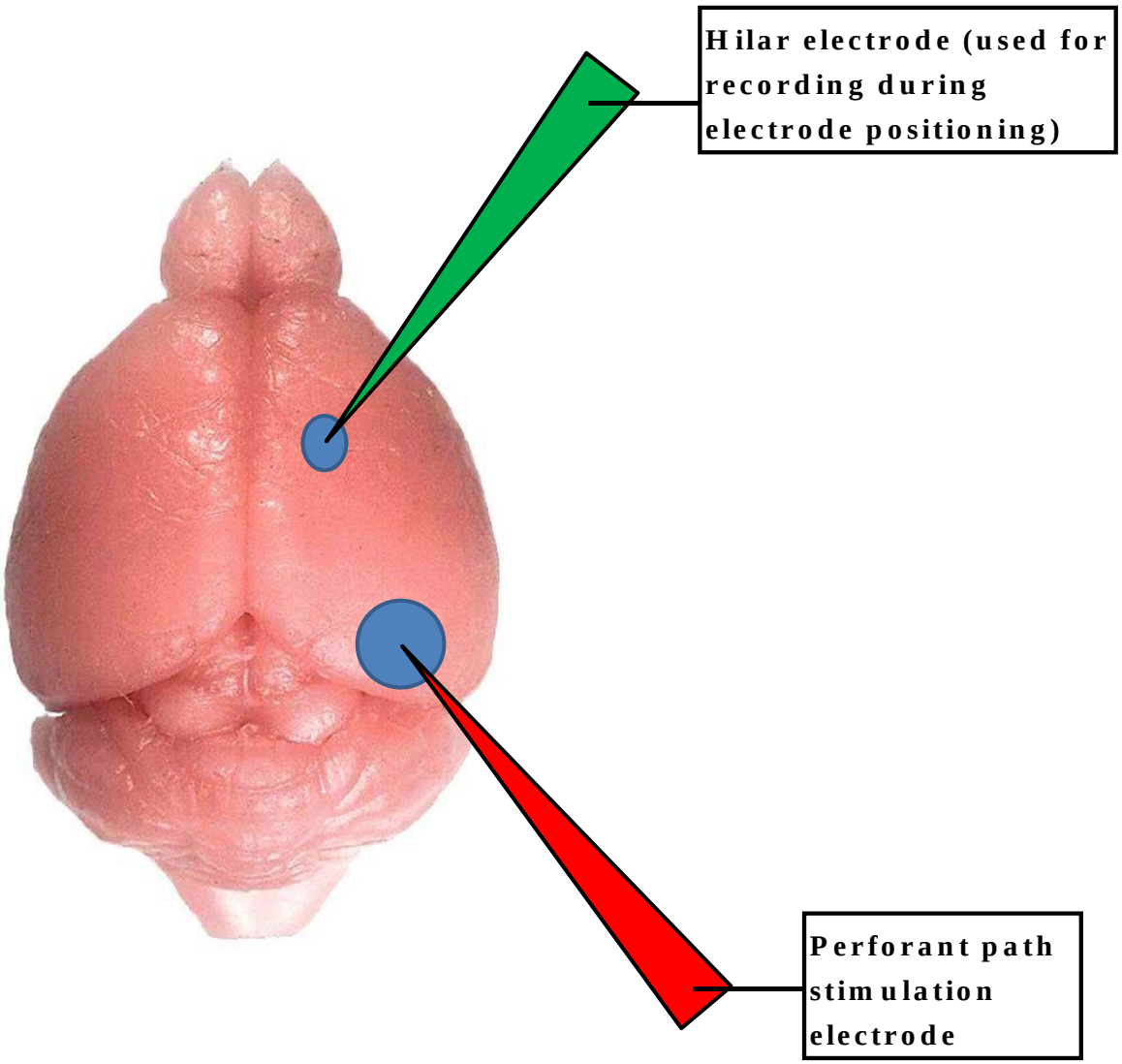

Figure 4: Positioning of the electrodes in the DG
Schematic view of the positions of the electrodes. A concentric bipolar electrode with a tip/shaft distance of 250µm was used for hilar stimulation. For the positioning it was used as a recording electrode while stimulating the PP with a concentric bipolar electrode with a tip/shaft distance of 500µm.

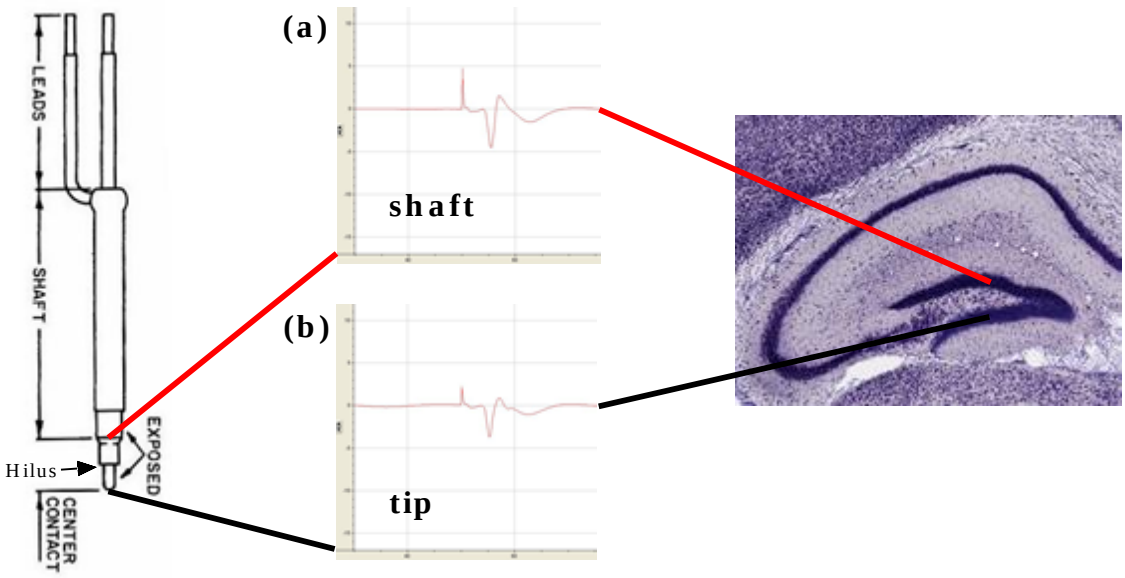

Figure 5: Positioning of the electrode in the DG with corresponding evoked potentials
Placement into the contralateral hilus by simultaneous recording from the tip and the shaft.
(a) shows recording from the shaft of the electrode. The laminar profile recorded at this position corresponds to the suprapyramidal GCL.
(b) shows recording from the tip of the electrode. The laminar profile recorded at this position corresponds to the infrapyramidal GCL.
The hilus is located between tip and shaft electrodes.

The electrode in the DG was then positioned by using its tip as a recording electrode to detect the stimuli generated by the stimulation electrode in the PP. Recordings were made in succeeding layers until a robust GC response was registered (suprapyramidal blade of the DG). Then the wires of the hilar electrode were switched so that the proximal part of the electrode could be used for recording. The electrode was then moved deeper into the tissue until again a robust GC response was registered. Finally, the wires of the hilar electrode were again switched to the initial situation so that again the tip of the bipolar electrode was used for recording. The depth of the bipolar electrode was accepted if the recording from the tip showed again a robust GC response (infrapyramidal blade of the DG). As a result of this careful calibration maneuver the stimulation maximum which is located approximately in the middle between tip and shaft was located in the hilus, which is the area of the MCs.

4.1.4 Electrophysiological Measurements

Recordings were made with a glass-electrode filled with 0.9% sodium-chloride solution and connected to a silver wire. The correct spot of recording was estimated based on the experience of former studies as well as a mouse brain atlas (Franklin and Paxinos,

1997). We were able to get a clear laminar profiles after EC-stimulation as well as hilar stimulation. The specific responses were compared to curves from published studies.

4.1.5 Histological Control of Lesion Quality

The ECL technique in mice was previously established by Dr. del Turco in our laboratory (Del Turco et al., 2003). For the in-vivo lesion experiments, which are part of this thesis, Dr. del Turco transferred this technique to the working group of Dr. Schwarzacher. For the control of lesion quality histological sections were stained with AChE by Dr. D. del Turco.

4.2 ANIMALS

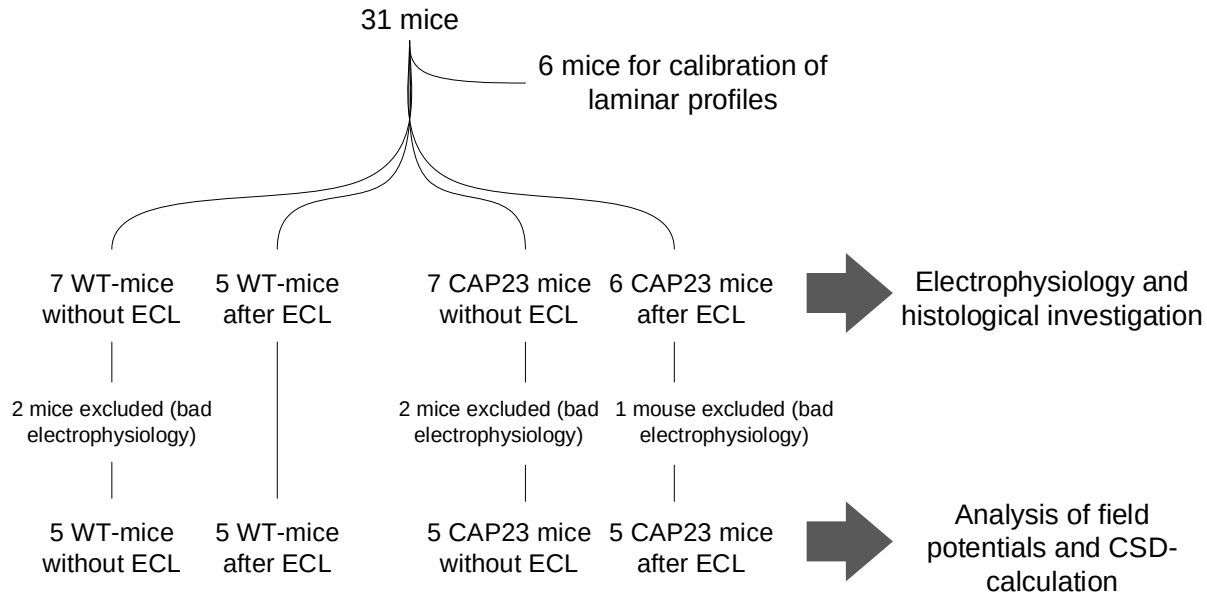

Figure 6: Overview of the animals used in this thesis
31 mice were included in this study. 6 mice were used for calibration of the laminar profiles. Of the remaining 25 mice 7 were wild-type mice without Lesion, 5 were wild-type mice after lesion, 7 were CAP23-overexpressing mice without lesion and 6 were CAP23-overexpressing mice after lesion. All mice underwent electrophysiology and histological investigation. All but 5 mice of each group underwent a detailed analysis of the FPs and a CSD-calculation.

Prior to the relevant experiments n=6 wild-type CB6F1 mice aged 12-16 weeks were used for calibration of laminar profiles. Experiments relevant for the study were performed on n=25 CB6F1 mice (Charles River Laboratories Germany, Sulzfeld, Germany) aged either 8 – 10 weeks for ECL or 12-16 weeks for electrophysiological measurements and housed under normal laboratory conditions. Experimental animals were divided into four groups: control animals and animals with unilateral ECL (Figure

6). Animals with ECL were allowed to survive for 4 – 6 weeks before undergoing electrophysiological measurements. All measured FPs were evaluated for signal quality. Amplitudes in GCL after stimulation of the PP $\geq$ 1mV were accepted and further analysis and CSD-calculations were performed. Five mice were excluded due to signal quality (two mice in each control group and one CAP23tg/ECL). All experiments were carried out in accordance with German laws governing the use of laboratory animals. All analyses were carried out on male age-matched littermates (12-16 weeks old mice).

4.3 SURGERY AND IN-VIVO ELECTROPHYSIOLOGY

The CAP23tg mice as well as their WT littermates were each divided in two groups. Mice belonging to a group were scrambled (experimenter blind to genotype) before ECL was performed.

4.3.1 Anesthesia

Anesthesia was performed as described in 4.1.1.

4.3.2 Transection of the PP (ECL)

Unilateral transection of the left PP was performed using a wire-knife (David Kopf Instruments, Tujunga, CA). The animals were fixed in a Kopf 1430 stereotactic head holder (David Kopf Instruments, Tujunga, CA, USA). Following anesthesia, the skin was cut using a sterile scalpel and the skull was exposed. The ECL was performed according to the protocol of Dr. D. del Turco (Del Turco et al., 2003). The lateral coordinate for lesion placement was estimated to be 2.5mm from the bregma. A small window was drilled directly above the transverse sinus, and the anterior/posterior coordinate was estimated +0.06mm from the approximate center of this landmark. The knife was rotated 15° axially and 10° in sagittal direction and was then placed -4.5mm ventral from the skull, extended 2.5-3mm, brought 4 mm dorsal, retracted, and removed from the brain. After the ECL, the skin was stitched and the mouse was kept in a warm surrounding until the anesthesia wore off.

Figure 7: Setup for ECL
Wire-Knife from David Kopf Instruments. The arrow indicates the blade. Picture taken from the website and with the permission of David Kopf Instruments (http://www.kopfinstruments.com).

4.3.3 Electrophysiological Measurements

For measurements either without ECL or 4-6 weeks after ECL, 12-16 weeks old mice from the above defined four groups were anesthetized and kept at 37°C. Anesthesia was performed as described above. All recordings were made with the experimenter blind to the genotype.

4.3.3.1 POSITIONING OF THE ELECTRODES

The stimulation electrodes were positioned as described in 4.1.3.

4.3.3.2 RECORDING

Recordings were made in the left hemisphere throughout the hippocampus and the DG in succeeding layers (1.7mm posterior and 1.0mm lateral to bregma), starting with CA1 stratum oriens and subsequently going deeper in steps of 50µm in z-axis. For stimulation, alternating impulses from contralateral PP and contralateral MCs were used. Recordings were made with a glass-electrode filled with 0.9% sodium-chloride solution and attached with a silver wire.

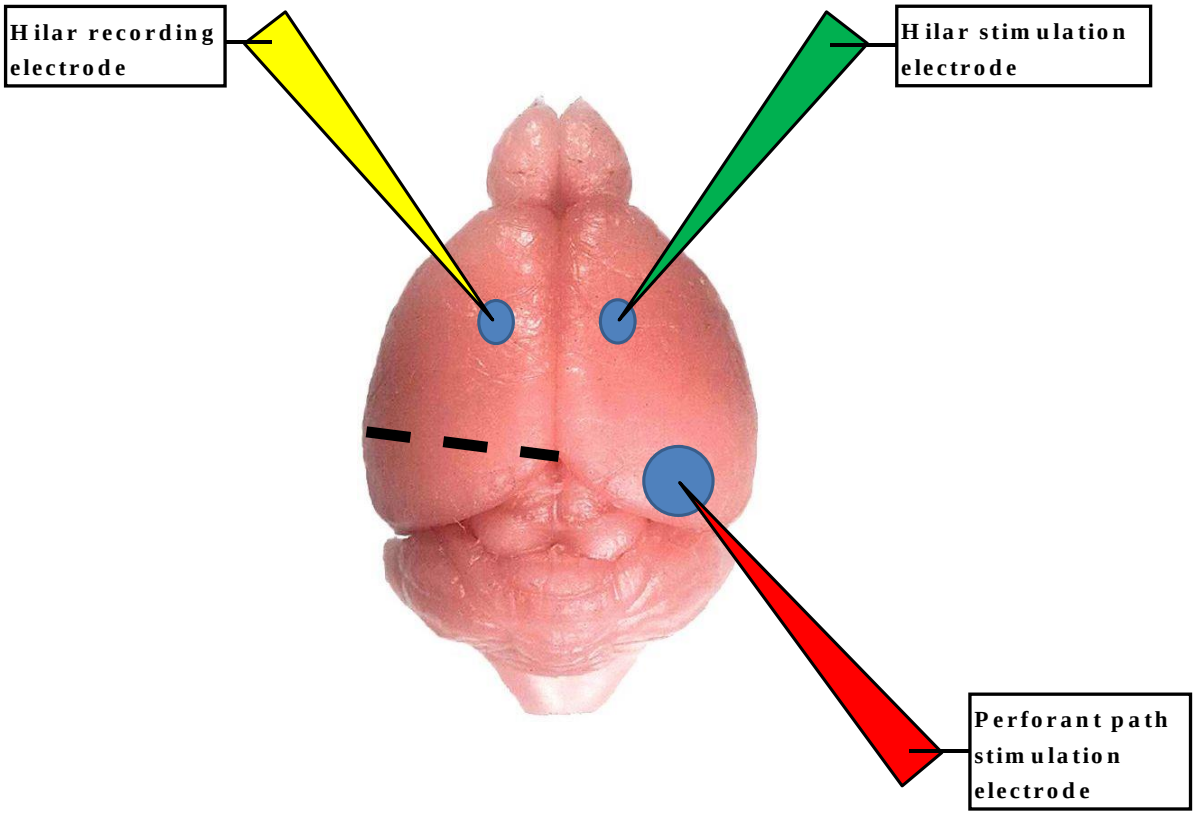

Figure 8: Schematic illustration of places of stimulation
Positions of stimulation- and recording electrodes. The black line marks the ECL.

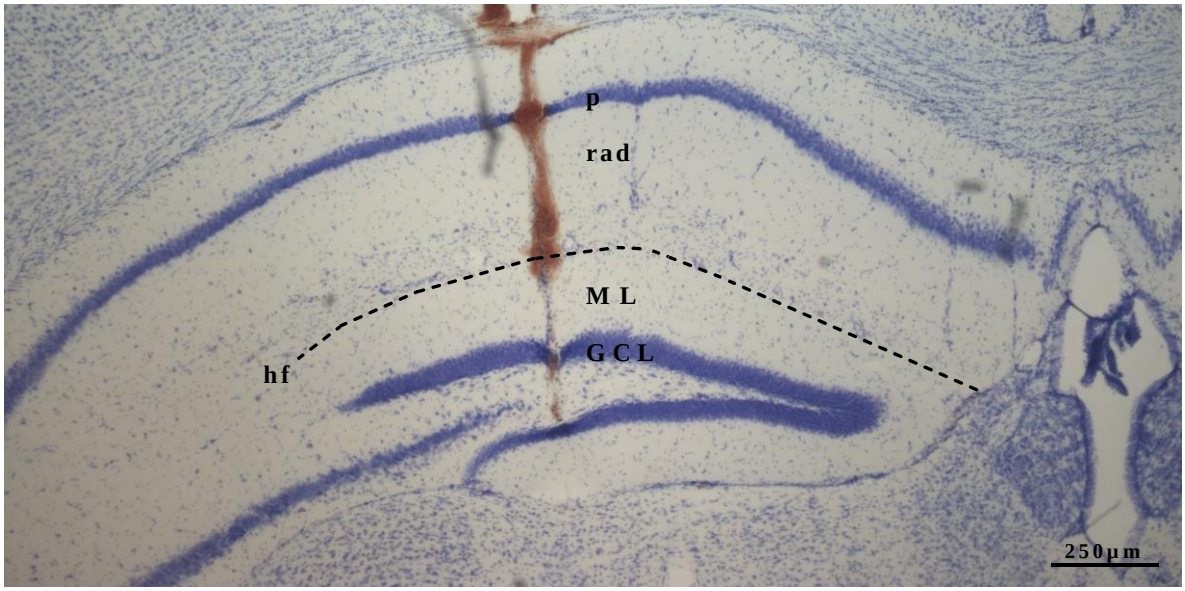

Figure 9: Trace of recording electrode
Hippocampus and DG in Nissl-staining. The red trace is the trace of the recording-electrode being inserted into the left DG. Abbreviations: p: *stratum pyramidale*; rad: *stratum radiatum*; hf: hippocampal fissure; ML: molecular layer; GCL: granule-cell layer

After the measurement of the laminar profiles we stimulated with a high-amperage monophasic stimulation with 1A of current intensity for 3s. This facilitated the identification of the electrode tip in Nissl-stained sections (Figure 10).

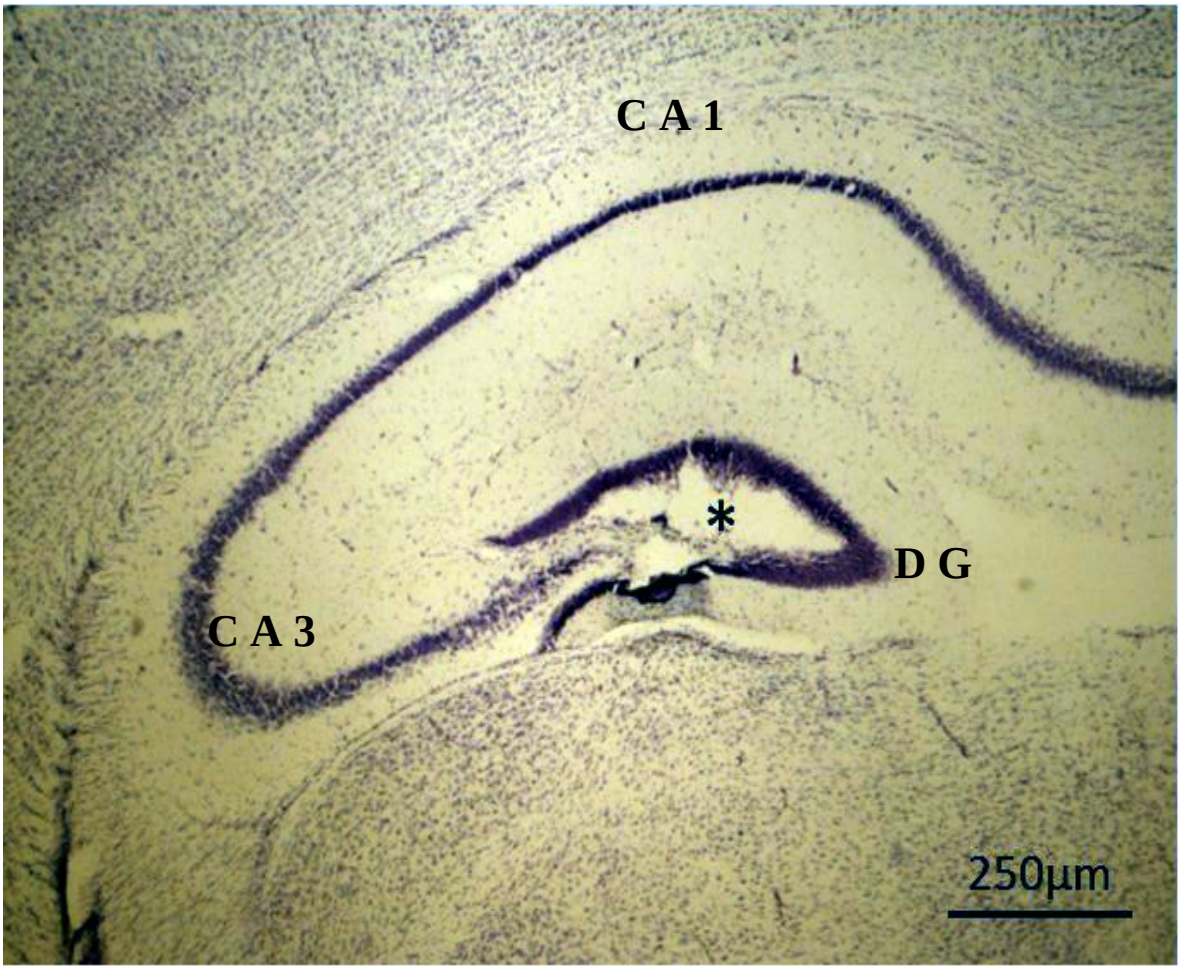

Figure 10: Control of electrode positioning
Nissl-stained section of hippocampal formation following 1A stimulation to identify the correct stimulation area. Abbreviations: CA1/CA3: CA1-/CA3-region; DG: dentate gyrus.

4.3.4 Perfusion and Immunohistochemistry

After the electrophysiological recordings the animal, while still under deep anesthesia, was transcardially perfused with 4% paraformaldehyde. The brain was removed and kept in 4% paraformaldehyde for 4-12h followed by washings in phosphate buffer. Coronal vibratome sections (50µm) were cut and stored in a cryoprotection solution at -20°C. Sections were stained mainly with Nissl (cresyl violet), especially in the area of

the electric stimulation in order to retrospectively ensure the correct position of the stimulation electrodes. Nissl staining was performed using standard protocols. Sections neighboring the sections containing the track of the recording electrode were used for immunohistochemical staining with calretinin to measure the width of the IML and the OML (Deller et al., 1999). Calretinin staining was performed by the team of Dr. D. del Turco using formerly published protocols (Del Turco et al., 2003). If an ECL had been applied on a mouse, some sections were stained immunohistochemically with AChE in order to evaluate the quality of the lesion, since AChE-positive fibers increase in density after lesion and correlate with the shrinkage of the OML (Lynch et al., 1972; Nadler et al., 1977a; Nadler et al., 1977b). AChE-staining was performed using established protocols as described in former studies by Dr. D. del Turco (Del Turco et al., 2003).

4.4 DATA-EVALUATION

4.4.1 Evaluation of the Electrophysiological Data

Electrophysiological responses were assessed in steps of 50µm and laminar profiles were generated for each source of stimulation, the contralateral hilar stimulation and the contralateral PP stimulation. Amplitudes of > 1mV were accepted. Furthermore the latency of response onset as well as the slope of the excitatory postsynaptic potential (slopeEPSP) were assessed. Finally CSDs were calculated for signals in the ML.

4.4.2 Latency-Shift Indicates Beginning of DG

The hippocampal fissure indicated the beginning of the ML. This was identified, as the response of CA1 came with a longer latency compared to the response of DG (see also chapter 5.2). This is due to the polysynaptic connection from the contralateral hilar MCs to the CA1 region compared to the monosynaptic connection to the ML. Stimulating the contralateral PP, we had a similar finding due to the pathway via the contralateral hilar MCs. So the latency-shift was used to identify the beginning of the ML.

4.4.3 Standardization of the Data

The amplitude of the population spike was defined as the average of the amplitude from the first positive peak (a) to the succeeding negative peak (b) and the amplitude from the negative peak (b) to the second positive peak (c): ([a-b] + [c-b])/2. For the analysis of the slope of fEPSPs, only the early component of the response was measured to avoid contamination by the population spike (Jedlicka P et al., 2011).

The measurement of slopeEPSP was plotted against the depth of the electrode. This approach yielded a series of laminar profiles. The depth measurement was standardized as follows: The beginning of the GCL, which was indicated by a clear source-appearance after the ML, was given the value 1 and the beginning of the ML, which was indicated by the shift of latency, was given the value 0. All other values were calculated relative to these distances. This relative approach (compared to an absolute approach using µm to measure depth) made it possible to disregard variations of individual mouse-brains or variations in the recordings (e.g. variations of insertion angles of the recording electrode).

The GCL-appearance and the shift of latency were measured by stimulating the contralateral PP. Depending on the quality of the signal the stimulation by the contralateral MCs was also considered, since the MC axons directly innervate the IML of the DG and the CA1-region is indirectly innervated. Furthermore, after fixation of the brains, the depths were measured histologically using a Nikon C1 Confocal microscope, which reconfirmed the position of the hippocampal fissure and the GCL.

The amplitude was also standardized: The maximum sink in the ML was defined as -100% and all other amplitudes were calculated in relation to that sink:

$$A = \frac{A_x}{A_{Min}} \times (-100\%)$$

4.4.4 Current Source Density

The calculation of the CSD was performed in collaboration Dr. R. Hartmann, Physiologisches Institut.

In the area of recording a one-dimensional CSD(z, t) was calculated as a function of depth z and time t by Dr. R. Hartmann using a second-order differential equation (Freeman and Nicholson, 1975; Nicholson and Freeman, 1975; Leung et al., 1990):

$$CSD(z;t) = \frac{\sigma[2\phi(z,t) - \phi(z+\Delta z,t) - \phi(z-\Delta z,t)]}{(\Delta z)^2}$$

Where $\phi(z,t)$ is the potential at depth z and time t and Δz is the distance (50µm) between two steps of recordings. Since area CA1 and the DG layers are organized in laminae, the x and y axes need not to be considered. Therefore a one-dimensional CSD(z, t) was considered to be sufficient. The acquired data sets were sufficiently noise free so that no spatial smoothing of the CSDs was necessary. The conductivity σ was assumed to be constant, and the CSDs were reported in units of V/mm² without using an actual value of σ.

4.5 STATISTICAL ANALYSIS

For statistical analysis GraphPad Prism was used (Version 6.01 for Windows, GraphPad Software, La Jolla California USA, www.graphpad.com). Gaussian distribution was assumed. Significant differences were assumed in the case of $p \leq 0.05$. Numbers of animals and the specific tests used for statistics are indicated in the figure captations.

5 RESULTS

5.1 RECORDING OF LAMINA-SPECIFIC PROFILES FOLLOWING STIMULATION OF THE CONTRALATERAL HILUS OR ENTORHINAL CORTEX

As described in the Methods, lamina-specific profiles were recorded after stimulating the contralateral hilar MCs or the contralateral PP. We recorded these profiles in the DG ipsilateral to an ECL (see also Figure 8) and in non-lesioned controls. Laminar profiles were assessed as described in 4.3.3.2. For the calibration of the laminar profiles n=6 CB6F1 WT mice were used.

The mean amplitudes recorded in each layer are summarized in Table 2. A trace sample can be seen in Figure 11. The mean values of the CSD-calculation for each layer are summarized in Table 3. A trace sample for the CSD-calculations is illustrated in Figure 12.

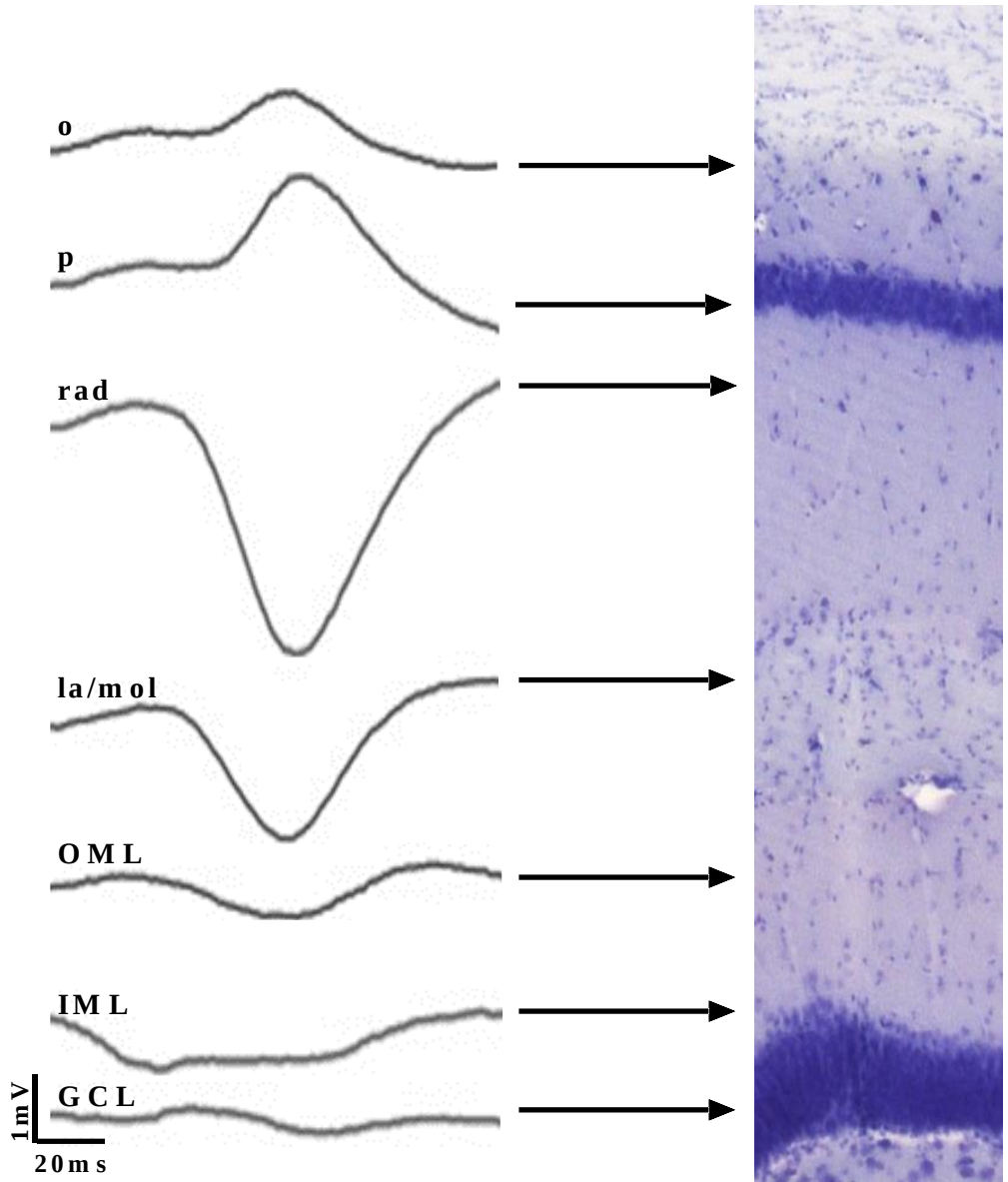

	Mean [mV]	SEM
Stratum oriens	0.86	0.17
Stratum pyramidale	0.98	0.39
Stratum radiatum	-0.77	0.55
Stratum lac. mol.	-1.36	0.52
OML	0.06	0.25
IML	-1.36	0.14
GCL	-0.69	0.21

Figure 11: Example of a laminar profile with a corresponding histological profile after hilar stimulation (commissural fibers)

Table 2: FPs following commissural stimulation

Figure 11 shows an example for a lamina-specific recording (laminar profile) of the hippocampus and the DG after hilar stimulation. A histological profile is shown on the right for orientation purposes [this was not the same animal]. Table 2 gives an overview of the mean FPs of each layer with corresponding SEM for n=6 wild-type animals. o: *stratum oriens*; p: *stratum pyramidale*; rad: *stratum radiatum*; la/mol: *stratum lacunosum-moleculare*; OML: outer molecular layer; IML: inner molecular layer; GCL: granule-cell layer.

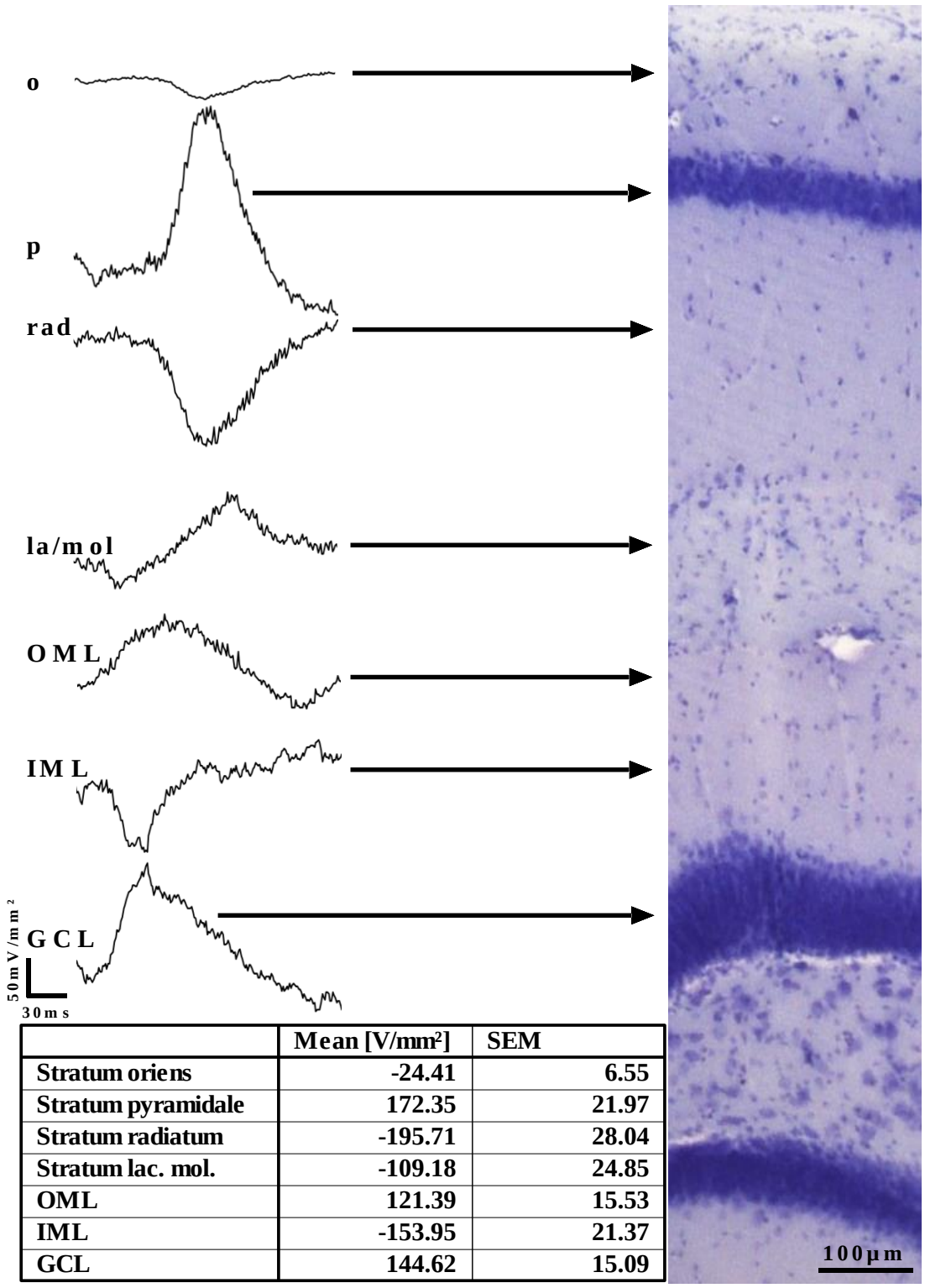

	Mean [V/mm²]	SEM
Stratum oriens	-24.41	6.55
Stratum pyramidale	172.35	21.97
Stratum radiatum	-195.71	28.04
Stratum lac. mol.	-109.18	24.85
OML	121.39	15.53
IML	-153.95	21.37
GCL	144.62	15.09

Figure 12: Example of a laminar profile (CSD-calculation) with a corresponding histological profile after hilar stimulation (commissural fibers)
Table 3: CSD-calculation following commissural stimulation
Figure 12 shows an exemple for a CSD-calculation series of the laminar profile shown in Figure 11 with a corresponding histological profile shown on the right. Table 3 gives an overview of the mean CSD-values of each layer with corresponding SEM for n=6 wild-type animals. o: *stratum oriens*; p: *stratum pyramidale*; rad: *stratum radiatum*; la/mol: *stratum lacunosum-moleculare*; OML: outer molecular layer; IML: inner molecular layer; GCL: granule-cell layer.

5.1.1 CA1-Region

Recordings started with the pipette entering *stratum oriens* of CA1. Even though *stratum oriens* is a dendritic layer, which contains basal dendrites of CA1 pyramidal cells, we saw a positive amplitude which arose from the neighboring *stratum pyramidale*. However, the CSD-calculation revealed a sink in this area. In *stratum pyramidale* we were able to show a positive amplitude (0.98mV) as well as a source-signal in the CSD-calculation (172.35V/mm²). In *stratum radiatum* we saw a negative amplitude (-0.77mV) as well as a prominent current-sink-signal in the CSD-calculation (-195.71V/mm²). *Stratum lacunosum-moleculare* contains the distal apical dendrites of the pyramidal cells. Unlike the other layers of area CA1, *stratum lacunosum-moleculare* is the layer in which afferents from the EC terminate. It contains a moderate amount of dendritic spines. Furthermore, a prominent inhibitory influence makes this layer hard to locate using electrophysiological measurements. Thus we were not able to locate this layer neither using FP measurement nor CSD-calculation. Nevertheless, the transition to the DG could be seen in the shift of latency (see below), so that this distal layer was estimated to be between *stratum radiatum* and the OML.

5.1.2 Dentate Gyrus

In the OML we saw a slightly positive FP (0.06 mV) as well as a current source in the CSD-analysis (121.39V/mm²). In the IML we saw a clear negative amplitude of the FPs (-1.36mV). The CSD-analysis revealed a current sink of -153.95V/mm². In the GCL, finally, the EPSPs generally lead to a positive slope and an action potential is generated. The electrophysiological response of dentate granule cells to the stimulation of the entorhinal cortex has been thoroughly investigated. It comprises of a positive slopeEPSP, which is interrupted by the population spike with a clear sink (Jedlicka et al., 2011). In contrast the stimulation of the commissural afferents does not generate a clear EPSP as the input to the IML is not only excitatory but also has a prominent inhibitory effect (Buzsáki and Eidelberg, 1981). Our findings are compatible with these previously published observations. The mean amplitude in the GCL was -0.69mV. However, there was a source visible in the CSD-calculation (144.6V/mm²).

In Figure 13 we graphically demonstrated the course of the FPs along the depth in the DG. As mentioned above it becomes obvious that the main input to the DG via the hilar MCs is in the IML as the IML shows the maximum of negativity. Furthermore, the slightly positive amplitude of the OML indicates the dipole effect in that area.

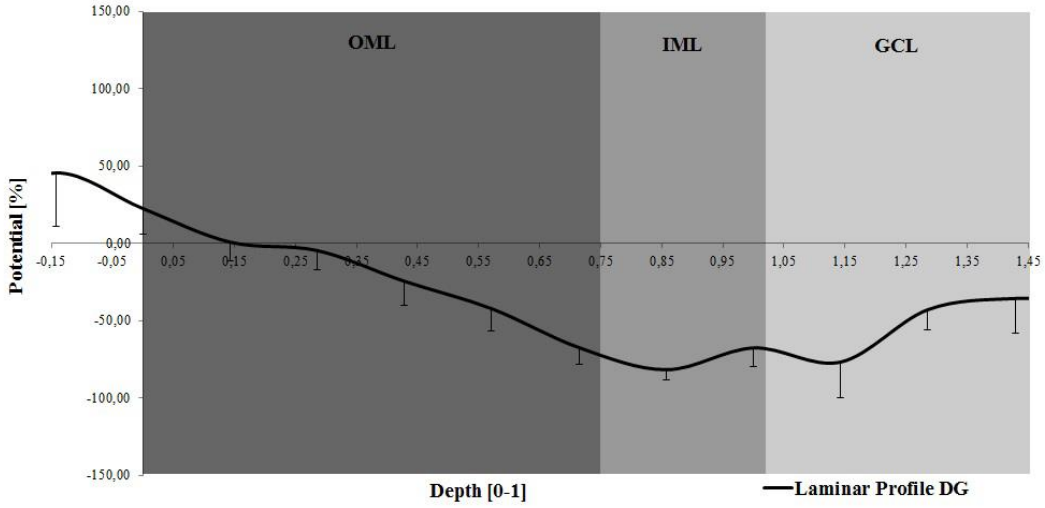

Figure 13: Graph of mean FPs of the DG
This graph shows the mean FPs of n=7 wild-type mice in the DG plotted against the relative depth. OML: outer molecular layer; IML: inner molecular layer; GCL: granule-cell layer.

5.2 SHIFT OF ONSET LATENCY FROM CA1 TO DG

In our experiments, we stimulated the EC as well as the hilar MCs of the hemisphere contralateral to an ECL and in non-lesioned controls. The recording of the evoked potentials was performed in the hippocampal formation contralateral to the stimulation. The recording electrode was lowered from area CA1 to the DG as described in the previous paragraph on the recording of laminar profiles.

5.2.1 Differences in Slope-Onset Latency in CA1 and DG

Stimulation of the hilar MCs contralateral to the recording side leads to a monosynaptic excitation of the GCL, thus generating a current sink in the IML and subsequently a current source in the OML. In contrast, stimulation of the contralateral EC reaches the DG disynaptically, since this stimulation is either relayed via the granule cells and hilar MCs (two synapses) or via an entorhino-entorhinal commissural projection to the

ipsilateral EC and from there to the DG (two synapses; does not apply to mice after ECL). Downstream to the DG the stimulus reaches CA1 via CA3 and the SC system (Blackstad, 1956, 1958; Megias et al., 2001; Buzsáki and Eidelberg, 1982). Thus, we hypothesized that there has to be a difference in the latency of the response to the stimulus between area CA1 (two synapses in the case of a hilar stimulation) and the DG (one synapse in the case of a hilar stimulation).

Indeed going stepwise deeper from area CA1 to the DG with the recording electrode, we detected a latency shift in n=5 mice for each of the four defined groups (Figure 14).

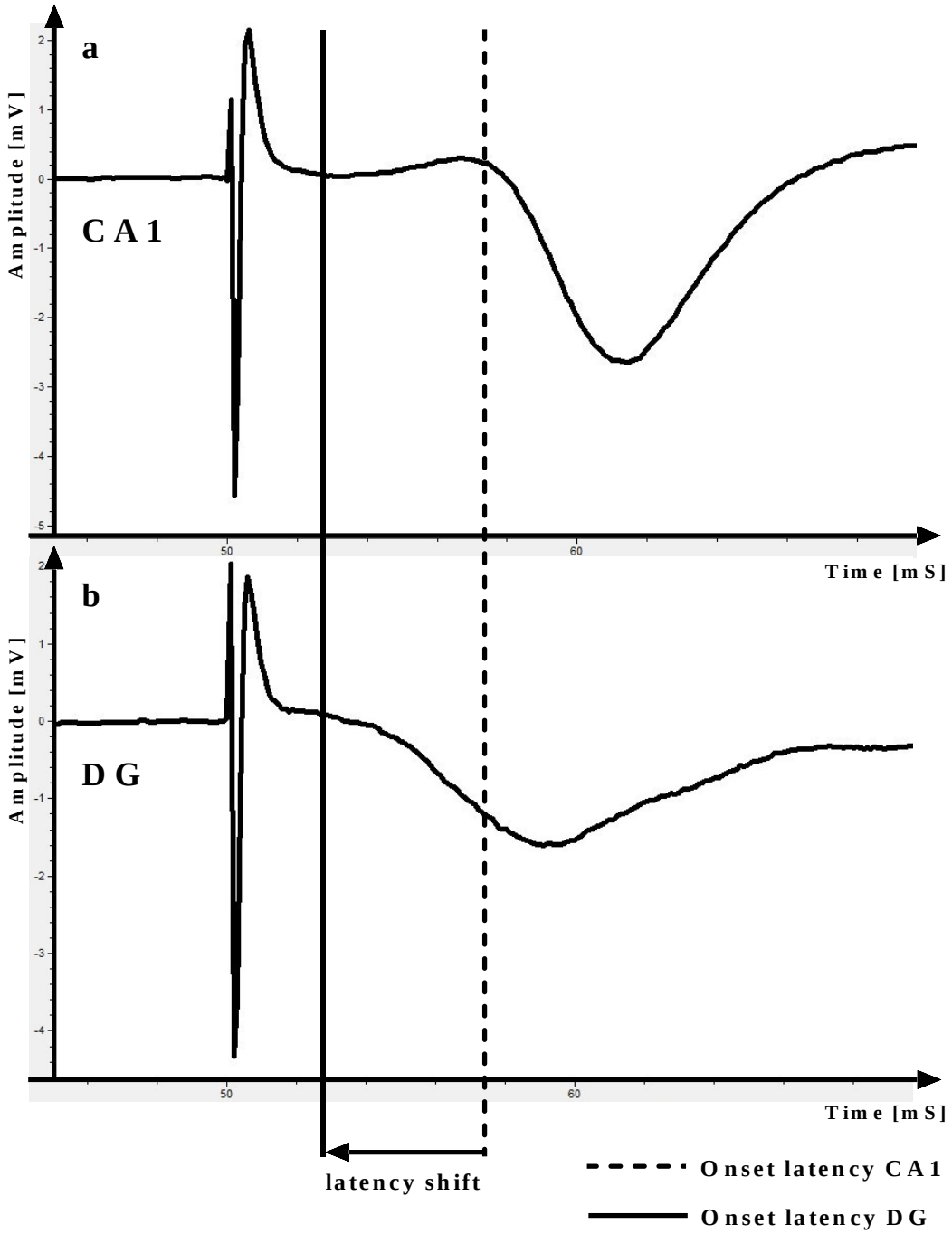

Figure 14: Sample trace indicating the latency shift
This figure shows a sample trace indicating the shift of response onset latency. a: recording in CA1; b: recording in DG. The turning point of the curve is used to identify the beginning of the response to the stimulus. The response latency is measured from the beginning of the stimulus artifact to the slope onset. Abbreviations: CA1: CA1-region; DG: dentate gyrus.

The main results are summarized in Table 4, Figure 15 and in Figure 16. A Gaussian distribution was assumed and Student's t-test was used for statistical evaluation. The latency shift was from 6.91ms to 3.96ms in WT mice without ECL, 6.31ms to 4.01ms in WT mice with ECL, 7.93ms to 4.98ms in CAP23tg mice without ECL and 6.35ms to

5.07ms in CAP23tg mice with ECL. There was a significant shift in all groups ($p < 0.01$) except for the CAP23tg mice with ECL ($p = 0.07$). However, even in the latter group a clear trend was visible.

	Mean time to CA1 [ms]	SEM	Mean time to DG [ms]	SEM	p-value
WT	6.91	0.50	3.96	0.35	< 0.01
WT/ECL	6.31	0.51	4.01	0.32	< 0.01
CAP23	7.93	0.28	4.98	0.62	< 0.01
CAP23/ECL	6.35	0.56	5.07	0.28	0.07

Table 4: Overview of the response onset latencies to CA1 and DG.
This table shows the mean response onset latencies to CA1 and DG depending on the genotype and the lesion status with n=5 for each group. For statistical analysis the students t-test was used.

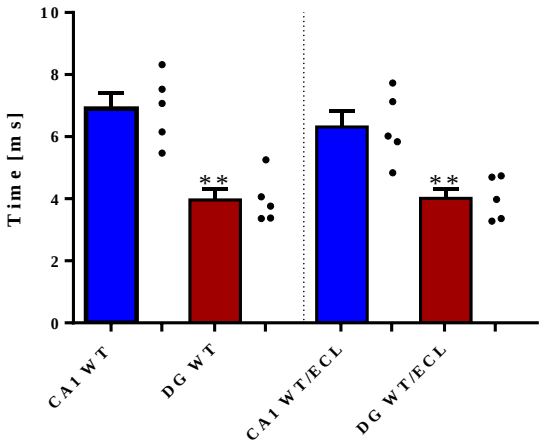

Figure 15: Mean response onset latencies for WT-mice without and with ECL
This diagram shows the response onset latencies to CA1 and DG in WT-mice without (n=5) and with ECL (n=5). In both groups there is a significant latency shift.

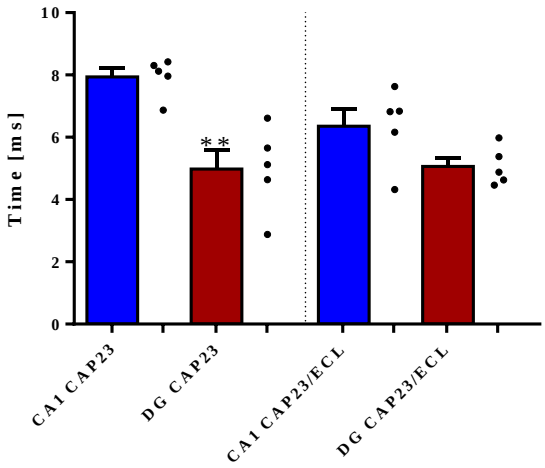

Figure 16: Mean response onset latencies for CAP23tg-mice without and with ECL
This diagram shows the response onset latencies to CA1 and DG in CAP23tg mice without (n=5) and with ECL (n=5). In the unlesioned mice there is a significant shift. In the lesioned mice a trend is visible, which did not reach statistical significance.

The latency shift was used during the recordings to identify the hippocampal fissure, which divides area CA1 from the DG. In area CA1 we observed a long latency, as

shown in Figure 14a, whereas in the DG the latency was significantly shorter, as shown in Figure 14b.

To verify this interpretation of the latency shift, we correlated our electrophysiological findings with brain anatomy and performed histology. In these sections we measured the distance from the brain surface to the hippocampal fissure and compared this value with the value obtained during the electrophysiological recordings, i.e. the depth of the electrode in the brain. The main results are summarized in Table 5. There was no statistical difference in the histological and the electrophysiological measurement of the hippocampal fissure. An example for our histological measurement can be seen in Figure 17. Though not significantly different some inaccuracies between both methods of defining the fissure derive from the definition of the beginning of the brain surface in the electrophysiological investigation (visually determined) as well as some shrinkage following fixation of the tissue.

	Histology [µm]	SEM	E´phys [µm]	SEM
WT	1647.13	54.96	1585.71	52.00
WT pECL	1604.74	30.59	1530.00	37.42
CAP23	1615.22	61.89	1735.71	87.09
CAP23 pECL	1606.19	71.19	1662.50	61.83

Table 5: Mean histological and electrophysiological depth of the hippocampal fissure
The table shows the mean histological and electrophysiological depth of the hippocampal fissure for each group (n=5 for each group). There is no statistical significant difference between these two methods of locating the hippocampal fissure in the above defined four groups.

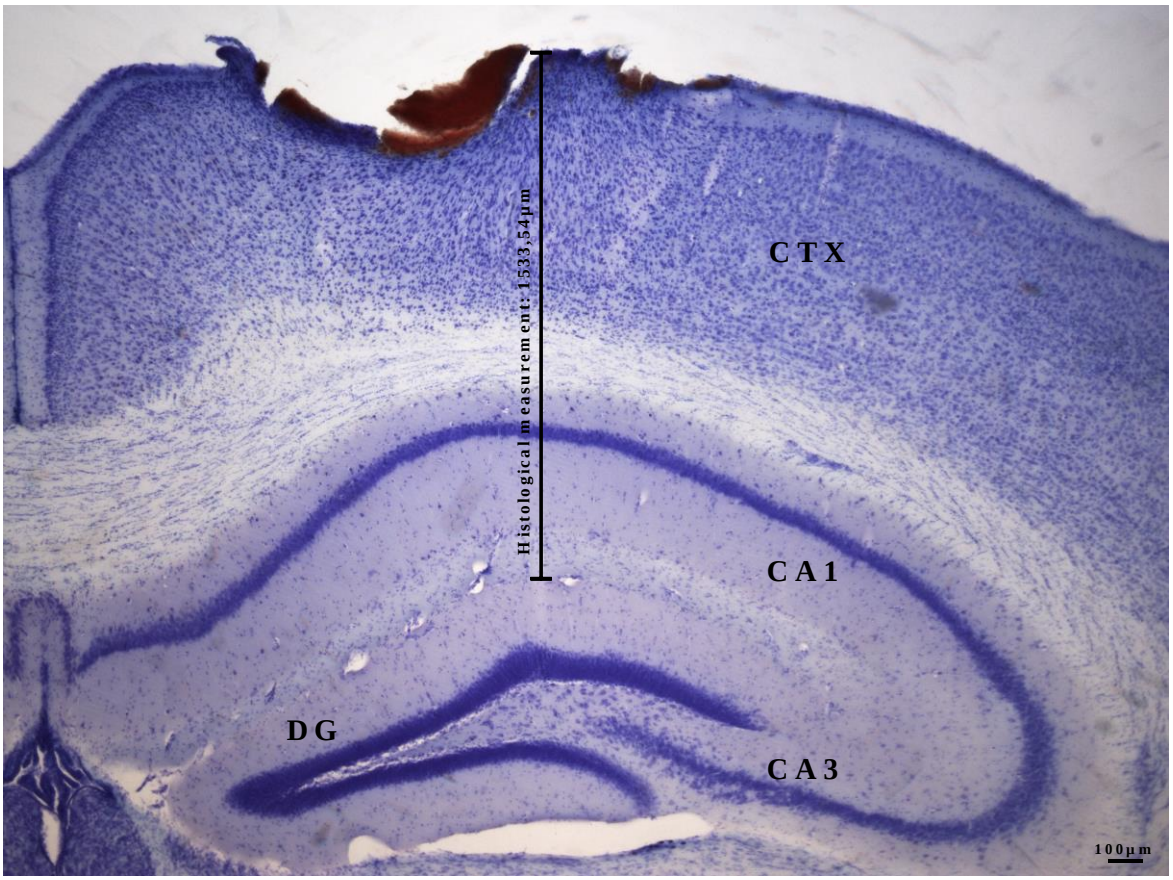

Figure 17: Histological measurement of the depth of the hippocampal fissure
This picture shows the histological measurement of the depth of the hippocampal fissure from the brain surface. Abbreviations: DG: dentate gyrus; CA1/3: area CA1 and area CA3, respectively; CTX: cortex.

5.3 THE DENERVATED DG SHOWS SHRINKAGE AFTER ECL

As previously described a denervation of the OML occurs after ECL in the mouse, which can be visualized using staining for AChE (Del Turco et al., 2003). This is due to the fact that the PP projects to the distal part of the ML and denervation leads to shrinkage of this layer (Phinney et al., 2004). These changes can also be used to control for lesion quality. Thus, we performed AChE- or and Nissl-staining of the hippocampus of mice after the electrophysiological recordings (Figure 18). In the AChE- and Nissl-stained sections of control and lesioned mice we measured the width of the molecular layer and determined the shrinkage of the DG following ECL.

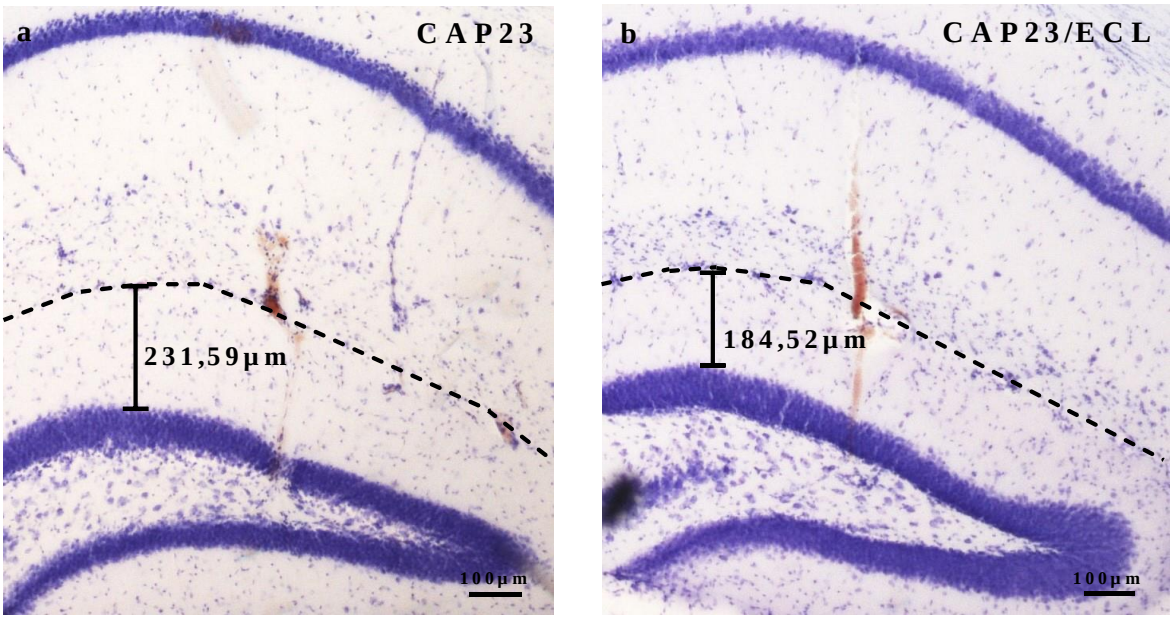

Figure 18: Hippocampus and DG of a CAP23tg mouse without and with ECL
The picture on the left (a) shows a CAP23tg mouse without a lesion. The ML has a width of 231.59µm. In comparison the picture on the right (b) shows a CAP23tg mouse 4-6 weeks after lesion. The width of the ML is only 185.52µm. The sections are Nissl-stained.

We measured the ML on sections stained for Nissl or AChE and compared the width of the ML of mice with and without ECL. We detected a shrinkage of the ML in the mice with ECL regardless of their genotype (Figure 19). The mean width of the ML in mice without ECL was 211.48µm (SEM=4.27µm) for WT mice and 224.31µm (SEM=6.92µm) for CAP23tg mice, while with ECL it was 173.94µm (SEM=13.56µm) for WT mice and 174.29µm (SEM=14.67µm) for CAP23tg mice, respectively. Both genotypes showed a clear trend of shrinkage after ECL was clearly visible. But only CAP23tg mice had a statistical significant shrinkage after ECL. For statistical investigation a one-way ANOVA with Sidak`s multiple comparison test was used. Gaussian distribution was assumed.

	Mean [µm]	SEM [µm]
WT	211.48	4.27
WT/ECL	173.94	13.56
CAP23	224.31	6.92
CAP23/ECL	174.29	14.67

Table 6: Mean ML-width
This table shows the mean width of MLs for WT mice without (n=7) and with ECL (n=5) as well as CAP23tg mice without (n=7) and with ECL (n=6).

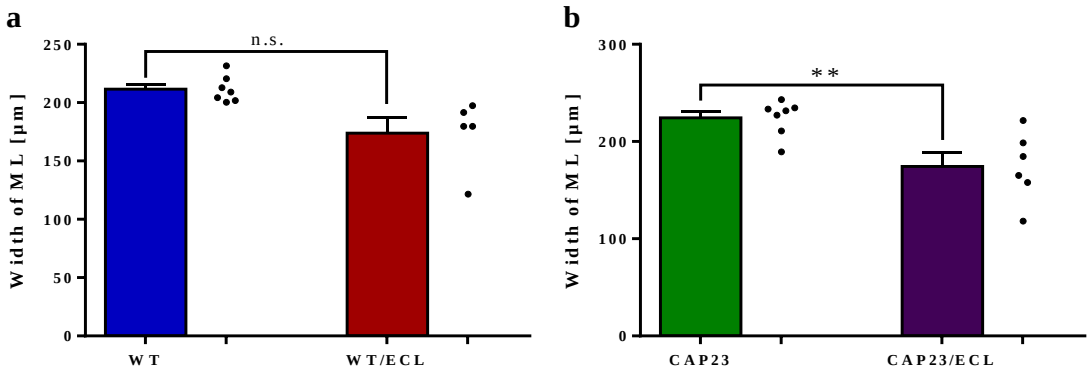

Figure 19: Shrinkage of the ML after ECL
The columns show the width of the ML for WT mice (a) without (n=7) and with ECL (n=5) as well as CAP23tg mice (b) without (n=7) and with ECL (n=6). The width was measured in Nissl-stained sections or if after ECL, alternatively in AChE-stained sections. A shrinkage of the ML could be seen in both groups. While in CAP23tg mice this shrinkage was statistically significant, in WT-mice no statistical significance could be achieved. However, a trend is clearly visible. For statistical analysis one-way ANOVA with Sidak`s multiple comparison test was used.

5.4 IN THE OUTER MOLECULAR LAYER THERE IS AN ENHANCED SINK AFTER DENERVATION IN CAP23TG MICE

Following after denervation of the OML the denervated granule cell dendrites are reinnervated by axon collaterals coming from the MCs and sprouting from the IML to the OML (Del Turco et al., 2003). As CAP23 increases the sprouting of axon collaterals we speculated that this reinnervation is enhanced in CAP23tg mice and looked for electrophysiological correlates for such an enhanced sprouting response.

The effect of CAP23-overexpression has been described in earlier studies (see also 3.2.2). CAP23 is widely and abundantly expressed during development, maintained in some brain-structures in adults and upregulated during nerve regeneration (Caroni, 1997; Frey et al., 2000). It could be shown that CAP23 is closely related to GAP43 and both are intrinsic determinants of anatomical plasticity functioning by locally promoting subplasmalemmal actin cytoskeleton accumulation (Frey et al., 2000). An overexpression of CAP23 leads to a promotion of axonal sprouting in the adult mouse brain (Aigner et al., 1995; Caroni et al., 1997). It has not been investigated though what kind of effect this sprouting has on the network function.

The sprouting mossy cell axons which reinnervate the denervated GC dendrites are glutamatergic. This should lead to an enhanced sink, as shown in our CSD analysis (see also 4.4.4). We therefore hypothesized that an enhanced negative slopeEPSP in the region directly after the hippocampal fissure should occur indicating the sprouting of glutamatergic axons from the IML to the OML. The hippocampal fissure was identified as described above on the basis of the latency shift (see also 5.2).

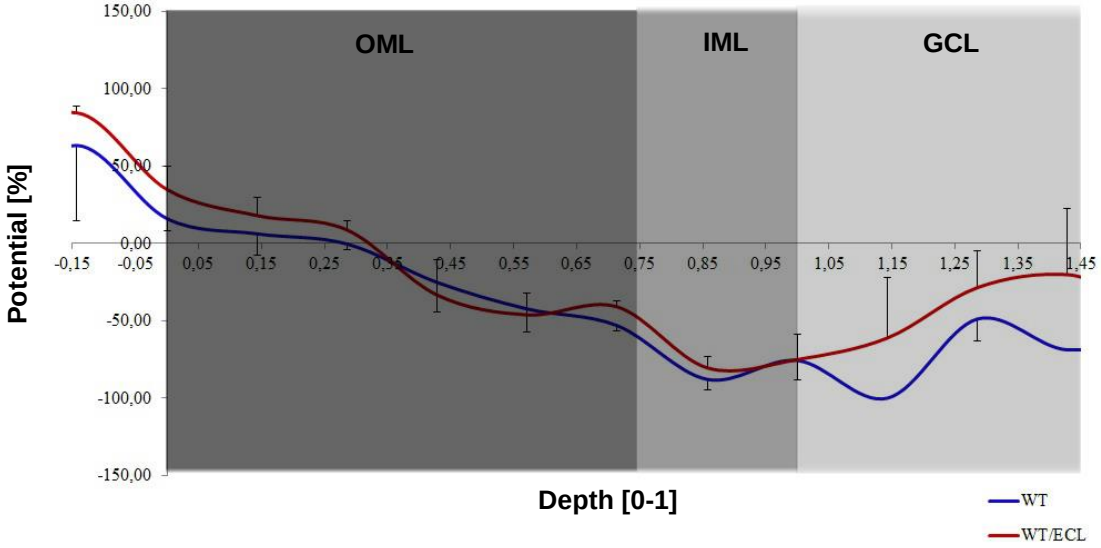

Figure 20: Graph of mean FPs of the DG of WT mice
This graph shows the mean FPs of WT mice without (n=5) and with ECL (n=5) in the DG plotted against the relative depth. There are no statistically significant differences.

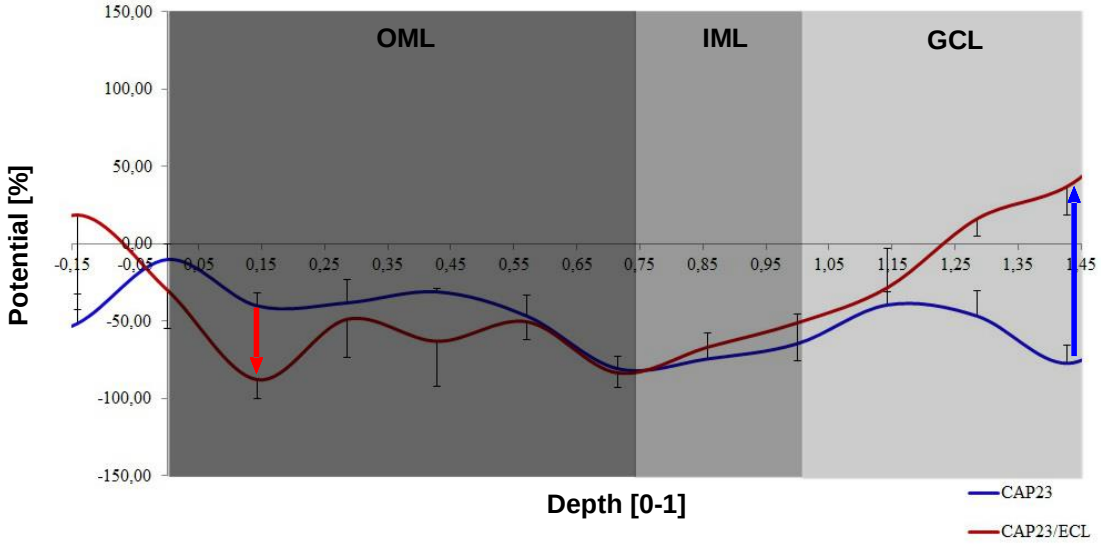

Figure 21: Graph of mean FPs of the DG of CAP23tg mice
This graph shows the mean FPs of CAP23tg mice without (n=5) and with ECL (n=5) in the DG plotted against the relative depth. There is a clear enhanced sink in the OML indicated by the red arrow. Furthermore, a hyperexcitation in the GCL is clearly visible, indicated by the blue arrow.

	Mean FP [%]	SEM	Mean CSD [mV/mm²]	SEM
WT	-15.24	8.84	-9.36	18.49
WT/ECL	-20.86	16.43	-7.54	17.00
CAP23	-31.39	13.58	-3.56	7.22
CAP23/ECL	-86.28	8.01	-85.07	29.39

Table 7: Mean FP and CSD values in the OML
This table shows the mean FPs and the mean CSD values in the OML in each group of mice (n=5 for each group).

The laminar profiles are illustrated in Figure 20 and Figure 21 and summarized in Table 7. We were able to show a significantly increased sink in the OML of CAP23tg mice after ECL compared to those without ECL and also compared to the WT mice after ECL (Figure 22). For statistical analysis we assumed Gaussian distribution. A one-way ANOVA with Sidak's multiple comparison test was used.

5.5 AFTER REINNERVATION OF THE OML THE GRANULE-CELLS BECOME MORE EXCITABLE IN CAP23TG MICE

As described before we compared the laminar profiles of the four groups not only in the OML, but also in the IML and the GCL. There was no significant difference in the

four groups in the IML (Figure 23). This is not surprising though, because by denervating the OML and after reinnervation by axon-collaterals we would not expect any change in the density of dendrites and axons in the IML.

Yet, we found a highly significant increase in excitability in the GCL (Table 8 and Figure 24). Stimulating the contralateral MCs we measured a positive FP of 74.36% in the CAP23tg mice after ECL while the litter mates without ECL and also the WT mice with or without ECL had a negative FP indicating a sink. For statistical analysis one-way ANOVA with Sidak's multiple comparison test was used.

	Mean FP [%]	SEM
WT	-32.60	11.03
WT/ECL	-15.61	20.02
CAP23	-64.29	17.52
CAP23/ECL	74.36	9.57

Table 8: Mean FPs in GCL
The table shows the strength of FPs in the GCL. There is a statistical highly significant source in the GCL of the CAP23tg mice after the ECL compared to the unlesioned mice of the same genotype ($p<0.0001$) as well as to the lesioned WT mice ($p<0.001$). For statistical analysis one-way ANOVA with Sidak`s multiple comparison test was used.

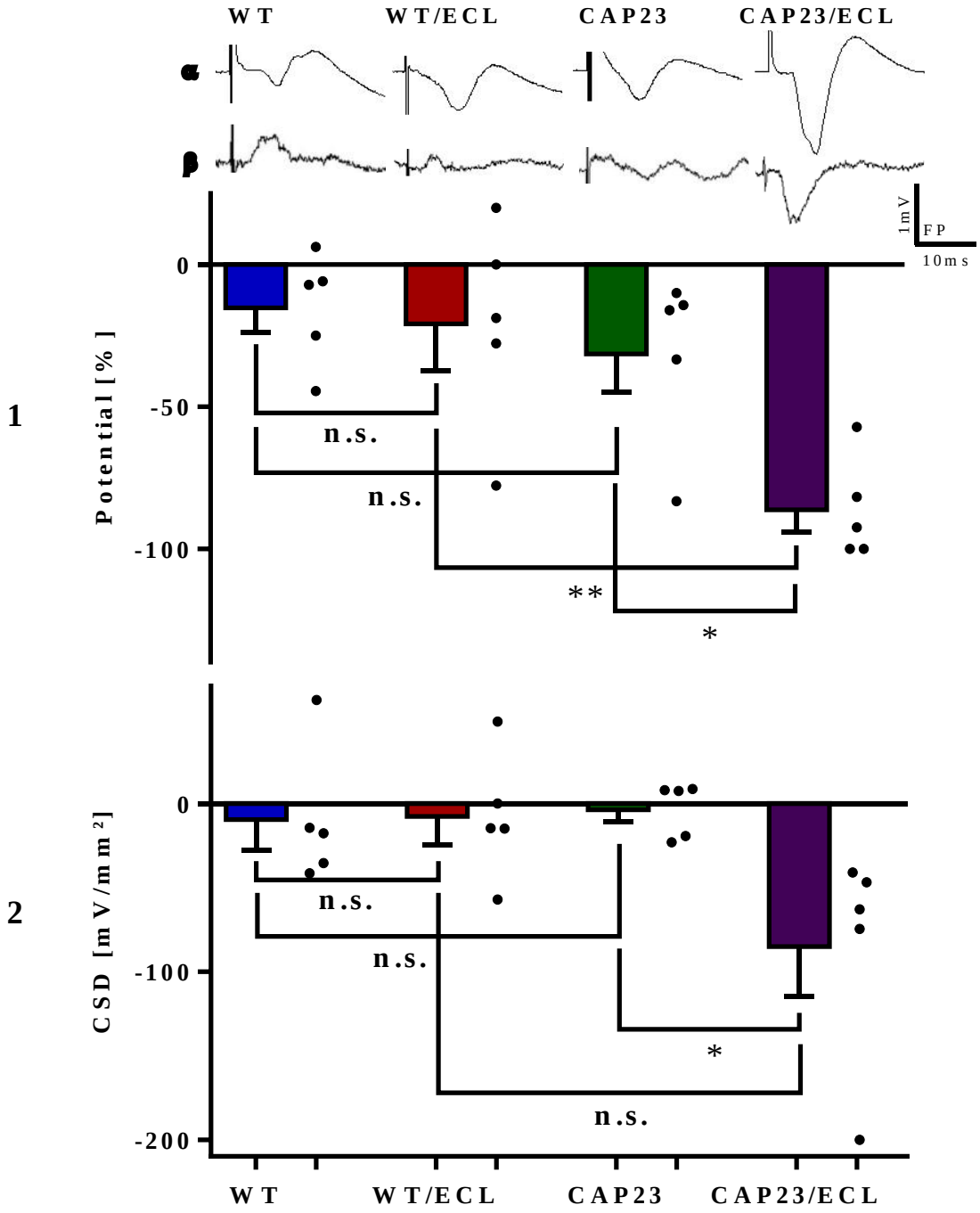

Figure 22: Average stimulus-induced FPs and calculated CSDs in the OML
This figure shows the stimulus-induced FPs and calculated CSDs in the OML for the four groups. The FPs are displayed as the average of the ratio on the maximal sink of each mouse. The bars in 1 show the FPs in the OML stimulated by the contralateral hilar MCs. Typical recordings of the FPs are shown in the plots in α. The bars in 2 show the average of the CSD-calculations in the OML. Typical CSD-traces are shown in the plots in β. Stimulus-artifacts are truncated. An enhanced sink can be seen in the CAP23tg mice after ECL. N=5 for each group. For statistical analysis one-way ANOVA with Sidak's multiple comparison test was used.

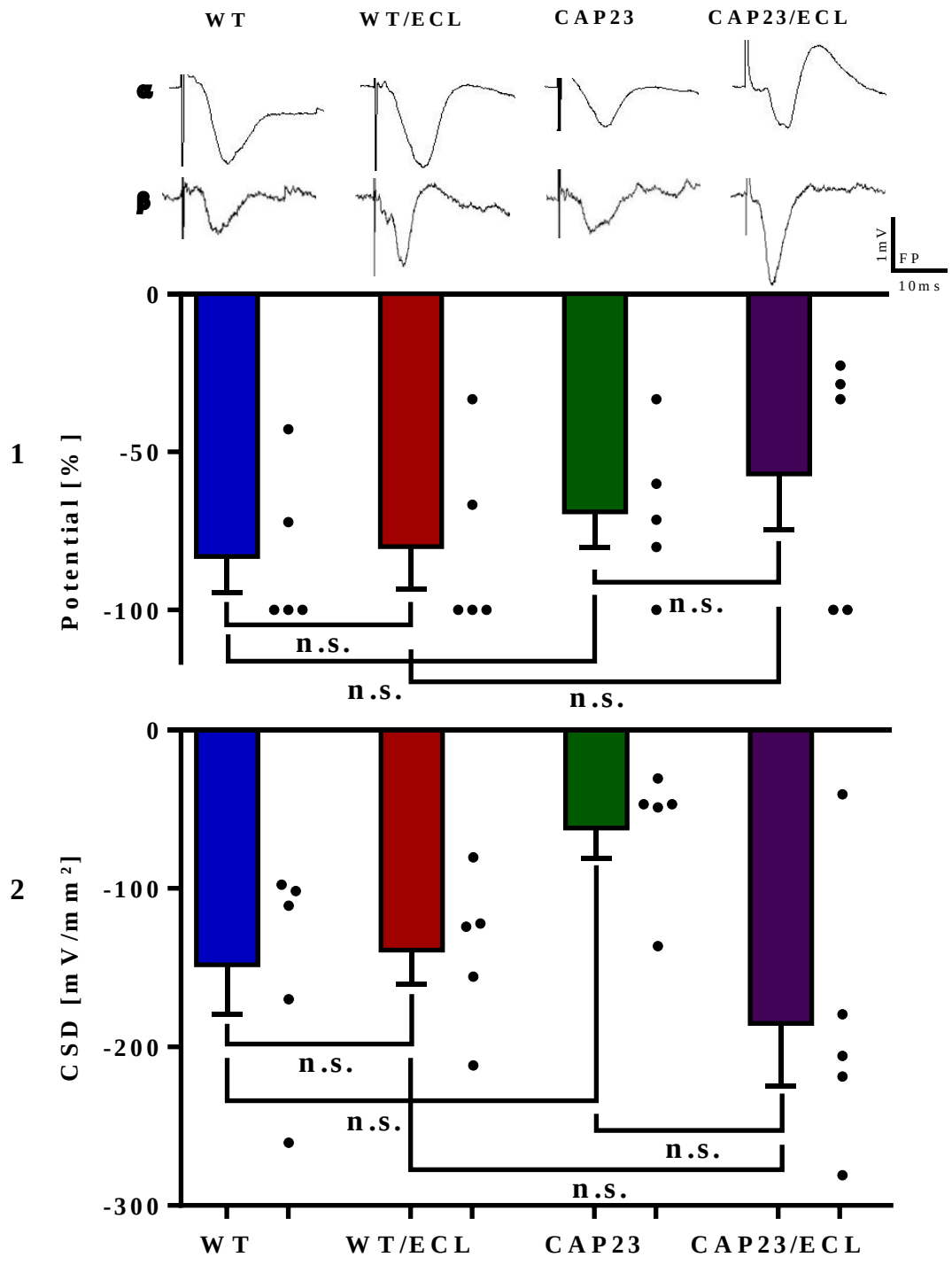

Figure 23: Average stimulus-induced FPs and calculated CSDs in the IML
This figure shows the stimulus-induced FPs and calculated CSDs in the IML for the four groups. The FPs are displayed as the average of the ratio on the maximal sink of each mouse. The bars in 1 show the FPs in the IML stimulated by the contralateral hilar MCs. Typical recordings of the FPs are shown in the plots in α. The bars in 2 show the average of the CSD-calculations in the IML. Typical CSD-traces are shown in the plots in β. Stimulus-artifacts are truncated. There is no statistical difference in each group. N=5 for each group. For statistical analysis one-way ANOVA with Sidak's multiple comparison test was used.

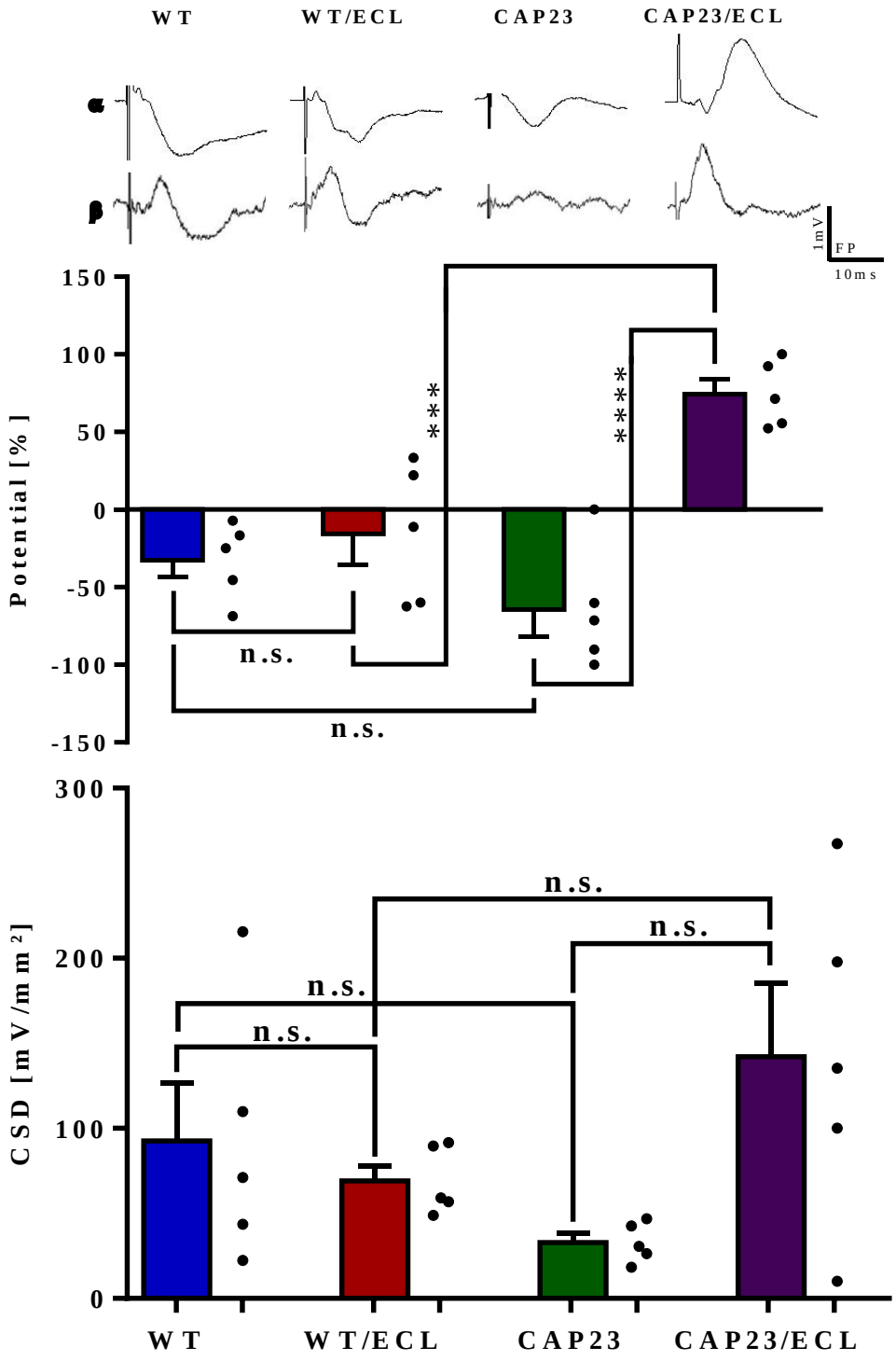

Figure 24: Average stimulus-induced FPs and calculated CSDs in the GCL
This figure shows the stimulus-induced FPs and calculated CSDs in the GCL for the four defined groups. The FPs are displayed as the average of the ratio on the maximal sink of each mouse. The bars in 1 show the FPs in the GCL stimulated by the contralateral hilar MCs. Typical recordings of the FPs are shown in the plots in α. The bars in 2 show the average of the CSD-calculations in the GCL. Typical CSD-traces are shown in the plots in β. We were able to show a highly significant excitation in the FPs. However, the CSD-calculation was able to show a source in all groups in the GCL, so that statistical significance could not be achieved. Stimulus-artifacts are truncated. N=5 for each group. For statistical analysis one-way ANOVA with Sidak's multiple comparison test was used.

6 DISCUSSION

Denervation of brain areas is a widespread consequence of brain injury. Denervated brain regions reorganize and remodel their connections. How this remodelling affects the ability of brain regions to process information is understood poorly. In our study, we used a classical in-vivo-lesioning model (entorhinal cortex lesion in vivo in mice) to study this phenomenon using extracellular electrophysiological recording methods. In addition to using wildtype mice, we also studied changes in CAP23tg mice, which show an enhanced sprouting response after a lesion. This way we were able to study functional changes in a denervated brain region under conditions with normal (wildtype mice) and enhanced sprouting (CAP23tg mice).

Our main findings can be summarized as follows:

1. The hippocampal fissure can be reliably identified using the shift of response onset latency (“latency-shift”) during in vivo recordings.
2. CAP23tg mice with an ECL show an increased current sink in the outer molecular layer of the dentate gyrus. This could be the electrophysiological correlate of the enhanced collateral sprouting response seen in CAP23 transgenic mice with ECL.
3. Based on FP-recordings dentate granule-cells of CAP23tg mice become hyperexcitable after ECL.

We conclude from these findings that there is a significant sprouting of axon collaterals in CAP23tg mice following ECL leading to a reinnervation of denervated dendrites in the OML. This sprouting is detectable in electrophysiological measurements in the form of a broader sink signal. An enhanced sprouting of glutamatergic fibers, i.e. glutamatergic commissural/associational mossy cell axons, may result in the hyperexcitability of granule-cells in CAP23tg mice. These functional changes occurring in the reorganized dentate gyrus need to be taken into account when considering therapeutic approaches aimed at enhancing the denervation-induced sprouting response.

6.1 ELECTROPHYSIOLOGICAL RECORDINGS OF LAYER-SPECIFIC PROFILES IN THE HIPPOCAMPUS AND THE DENTATE GYRUS OF MICE

In this study we recorded laminar profiles with a single-channel electrode. Such laminar profiles have been previously described by others following ipsilateral PP stimulation (Kleschevnikov and Routtenberg, 2003; Liu and Bilkey, 1997). Kleschevnikov and Routtenberg (2003) also showed laminar profiles after stimulation of the A/C pathway (Kleschevnikov and Routtenberg, 2003).

6.1.1 Laminar Profile of the Hippocampus

In earlier studies Buzsáki and Eidelberg (1981) demonstrated that the commissural and associational input to CA1 can excite CA1 pyramidal cells. They reported that both pathways terminate on apical as well as basal dendrites of CA1 neurons. In their report they noted that commissural input was more efficient in *stratum oriens*, whereas associational input via the SCs was more efficient in *stratum radiatum* (Buzsáki and Eidelberg, 1981). In *stratum lacunosum-moleculare* afferents originating from the EC layer III pyramidal neurons (Blackstad, 1958; Megias et al., 2001) terminate, which play only a minor role in our stimulation protocol. Of note, this projection has been recently re-investigated and new data on the anatomy and function of the EC-CA1 projection has emerged (Masurkar et al., 2017).

In line with the previous reports, our FP-recordings showed a sink in *stratum oriens* and *stratum radiatum* in the CSD-calculation. However, a clear negative FP could only be shown in *stratum radiatum*. A negative FP in *stratum oriens* was not detected, even though we had expected one following activation of the contralateral hilar MCs due to subsequent activation of the SCs (Andersen et al., 1966; Blackstad, 1956; Gray, 1959; Hjorth-Simonsen, 1973; Megias et al., 2001; Storm-Mathisen and Fonnum, 1972). In fact, Kaibara and Leung (1993) had shown a small negative FP in *stratum oriens* in an earlier publication (Kaibara and Leung, 1993). However, the stimulation protocol used by these scientists directly stimulated the CA1-region. In contrast to this our protocol uses a stimulation of the contralateral hilus, not a direct stimulation of the CA1-region. Thus the activation is forwarded to the CA3-region by mossy fibers of the GCs, which

again leads to a bilateral excitation of the CA1-region via the SCs (Claiborne et al., 1986). This stimulation protocol is unlikely to result in a negative FP in *stratum oriens*, since this indirect stimulation of CA1 via the CA3-region is much stronger in *stratum radiatum* than in *stratum oriens* (Buzsáki and Eidelberg, 1982; Liu and Bilkey, 1997). Furthermore, a feed-forward inhibition has been described involving basket-cells of *stratum oriens* (Buzsáki and Eidelberg, 1982). These cells may reduce the excitation of the pyramidal cells by generating inhibitory postsynaptic potentials (IPSPs) in *stratum oriens*. This inhibition might also contribute to the absence of a negative FP in this layer.

In contrast to *stratum oriens* and *stratum radiatum* the pyramidal cell layer shows a current source. There are two major reasons for this: The first reason is that the neighboring layers contain current sinks, which generate a current source in the pyramidal cell layer. The second reason is that inhibitory influences on the pyramidal cells are located directly on the soma which leads to IPSPs at the cell-layer. The current source in the pyramidal cell layer has been described consistently in the literature (Kleschevnikov and Routtenberg, 2003; Leung et al., 1995; Brun et al., 1995; Liu and Bilkey, 1997).

6.1.2 Laminar Profile of the DG

The OML was considered the termination zone for excitatory afferents originating from the EC. Deller el al. (1995) could show, however, that inhibitory GABAergic neurons from the contralateral hilus also terminate in this layer (Deller et al., 1995b). This inhibitory input may play a role in the regulation of DG excitation as disinhibition of the DG facilitates seizures (Kobayashi and Buckmaster, 2003). Thus, stimulation of the contralateral hilar MCs leads to a slightly positive FP as well as a current source.

The IML is the proximal dendritic layer of the GCs. It contains mainly excitatory input arising from the MC axons from both hemispheres via the A/C pathway (Claiborne et al., 1990; Desmond and Levy, 1982, 1985). The IML has a negative FP and a current sink after activation of the MCs (Clusmann et al., 1994). The effect of the ECL on this layer shall be discussed later.

The GCL is the cell-layer of the DG. Like the pyramidal cell layer the GCL receives excitatory and inhibitory influences from several origins. However, the main electrophysiological response is primarily passive as the active sinks in the OML or the IML lead to a relative source in the GCL and a positive FP. This positive slope has also been reported by others (Jedlicka et al., 2011; Kleschevnikov and Routtenberg, 2003). The positive slope is more significant after stimulation of the PP. This is mainly due to the fact that stimulation of commissural fibers also activates feed-forward inhibition. It has been shown that the GCL is less excited after stimulation of the commissural pathway (Kleschevnikov and Routtenberg, 2003). However, the MCs themselves seem to have a strong excitatory effect on the GCs, which is compensated by the above mentioned strong inhibitory effect. Therefore, a spread of seizures originating from MCs might occur if GCs were disinhibited (Jackson and Scharfman, 1996; Kobayashi and Buckmaster, 2003).

6.2 THE LATENCY-SHIFT AS A RELIABLE METHOD TO IDENTIFY THE HIPPOCAMPAL FISSURE

The stimulation of CA1 is downstream to the stimulation of the DG originating either from the hilar MCs or from the contralateral EC (Blackstad, 1956, 1958; Buzsáki and Eidelberg, 1982; Megias et al., 2001). Thus we detected a latency-shift while lowering the recording electrode from area CA1 to the DG.

6.2.1 Latency-Shift After Stimulation of the Contralateral Entorhinal Cortex

There are two major pathways to the DG after stimulation of the contralateral EC: One is via commissural activation of the ipsilateral EC and one via the contralateral GCs and the AC pathway. In animals with ECL only the second pathway can be activated, since the ipsilateral PP is missing. Crossed fibers to the septal part of the contralateral DG coming from the EC are known in rats, rabbits, and cats (Goldowitz et al., 1975; Krug et al., 2001; Steward, 1980; Steward and Vinsant, 1978; van Groen et al., 2003). They seem to be essentially absent in mice (van Groen et al., 2002; Witter, 2007) and even very detailed analyses only revealed very few axons arising from the ipsilateral EC and terminating in the contralateral DG (van Groen et al., 2003). Thus, the

functionally relevant projection to the DG on the recording side stems from the hilar MCs of the contralateral hilus (Golarai and Sutula, 1996). These are activated by the mossy fibers of the GCs and have strong associational and commissural projections towards the IML of both hemispheres. Golarai and Sutula (1996) were able to show a current sink in the IML after stimulation of the contralateral EC, thus demonstrating that the stimulus can be relayed to the contralateral side via the commissurally projecting MCs. This current sink remained unchanged after ECL contralateral to the stimulation side, excluding any correlation with the entorhino-entorhinal pathway, while it vanished by ECL on the stimulation side, confirming the EC as the origin of the current sink (Golarai and Sutula, 1996).

On the other hand the innervation of the hippocampus by the contralateral EC has three possible routes: A mono-, di-, and polysynaptic pathway.

Layer III pyramidal neurons in the EC project to CA1 neurons via the PP. This input is also referred to as the temporo-ammonic path and is monosynaptic. It innervates only the distal apical dendrites in *stratum lacunosum-moleculare* (Blackstad, 1958; Megias et al., 2001). Some of the PP fibers innervating CA1 pyramidal neurons reach their targets in *stratum lacunosum-moleculare* via the temporo-alvear pathway (Deller et al., 1996a). Also arising from layer III is a crossed projection reaching CA1 and CA3 of the other hemisphere, albeit with a much lesser density (about 20%) (van Groen et al., 2003). This crossed projection seems to be heaviest in septal portions of the hippocampus and rapidly diminishes in strength at more temporal levels (van Groen et al., 2003). The monosynaptic input to the CA1- and CA3-region is expected to have a weaker influence on the initiation of a slope onset as the synapses formed by the PP in CA1 and CA3 are located in *stratum lacunosum-moleculare*, which is quite distant from the soma. Furthermore, relative to *stratum radiatum*, a greater proportion of synapses in *stratum lacunosum-moleculare* is formed on dendritic shafts, rather than spines (Megias et al., 2001). So the specific advantage of dendritic spines such as biochemical compartmentalization is considered as absent on these synapses (Andersen et al., 2007). Furthermore, the synapses from the PP terminating in *stratum lacunosum-moleculare* seem to have a much greater degree of inhibition by dopamine, serotonin and noradrenaline than the SC-synapses (Otmakhova and Lisman, 2000).

In sum, these PP afferents appear to be weak compared to afferents terminating on dendrites in *stratum radiatum*.

In the disynaptic pathway layer II pyramidal neurons of the EC project to CA3 neurons via the PP. This direct input to CA3 is again limited to the distal regions of the apical dendrites in *stratum lacunosum-moleculare* (Megias et al., 2001). CA3 pyramidal neurons themselves form the SC which projects to both sides of the brain and forms synapses on the apical dendrites in *stratum radiatum* and on the basal dendrites of *stratum oriens* (Blackstad, 1956; Hjorth-Simonsen, 1973; Schaffer, 1892; Storm-Mathisen and Fonnum, 1972).

The third and most prominent input to CA1 neurons arises from the axons of CA3-neurons activated by GCs (Claiborne et al., 1986). These CA3 neurons form the SC system which terminates on CA3 and CA1 dendrites in *stratum radiatum* of both hemispheres. Thus, MC axons activate GCs, which in turn activate CA3 neurons, which then activate CA1 pyramidal cells.

The immense network of interconnected recurrent collaterals of CA3 neurons has led to the belief that the CA3-region might play a role in memory storage and recall (Bennett et al., 1994; Rolls, 1996). Due to the high interconnectivity, however, the CA3 network is highly excitable and prone to seizure activity when inhibition is suppressed (Ben-Ari, 1985). Any significant excitation of CA3-neurons leads to an activation of the SC, thus activating the CA1-pyramidal neurons (Yeckel and Berger, 1990). Yeckel and Berger postulated a close interaction between these three pathways within the context of a feedforward excitation (1990).

Regarding the response onset, Yeckel and Berger (1990) consistently found a shorter onset latency in the DG than in the hippocampus (Yeckel and Berger, 1990). Paré et al. (1994) had the same finding in the guinea-pig brain in vitro (Pare and Llinas, 1994). Leung et al. (1995) had similar results even comparing the monosynaptic activations of the CA1-region and the DG-region (Leung et al., 1995), suggesting that the axons of entorhinal layer III cells that project to CA1 have to have a lower conduction velocity than the axons of the layer II cells that project to the DG. Leung estimated a conduction velocity of 2.7m/s to the DG and 1.7m/s to the CA1-region (1995).

6.2.2 Latency-Shift After Stimulation of the Contralateral Hilar Mossy-Cells

After stimulation of the contralateral hilar MCs, we were able to see a similar latency-shift as described before. As the projection from the contralateral EC is relayed to the DG via the commissurally projecting MCs, the response onset latency after stimulation of the contralateral hilus was similar to the contralateral EC.

The stimulation of the MCs leads to a monosynaptic activation of the DG, whereas the CA1-region is activated polysynaptically via mossy fibers, CA3 and the SCs. Golarai and Sutula (1996) have measured the latency of the response onset in the DG after stimulation of the contralateral hilar MCs with 3-5ms (Golarai and Sutula, 1996), which is in line with our findings. Despite of decades of research on the hippocampus there is no study investigating the response onset of CA1 after stimulation of the contralateral MCs. However, it becomes obvious that the activation of the CA1-region is always downstream to the activation of the DG, thus has a longer response onset latency compared to the DG. Our results revealed this shift in all mice with the average of the shift after stimulation of the contralateral MCs being 2.33ms $\pm$ 1.39ms.

In sum, both stimulations, i.e. stimulation of the contralateral EC and stimulation of the contralateral hilus, require activation of the commissurally projecting mossy cells. Since they both use the same pathways, a latency shift occurs under both stimulation conditions. Thus, under both stimulation conditions the latency shift can be used to distinguish CA1 from the DG.

6.2.3 Use of the Latency-Shift to Identify the Hippocampal Fissure

In our investigations it was necessary to locate the hippocampal fissure and thus locate the dorsal boundary of the OML in order to measure the difference of electrophysiological response before and after sprouting of axon collaterals. As far as we know this method has not been described yet in literature. However, considering our results the latency shift method seems to be a reliable approach to locate the ventral boundary of *stratum lacunosum-moleculare* and the dorsal boundary of the OML with electrophysiological methods. This allowed us to identify the location of the hippocampal fissure in our study.

6.3 DEGENERATION-INDUCED STRUCTURAL CHANGES IN THE DENTATE GYRUS OF WILDTYPE AND CAP23TG MICE FOLLOWING ENTORHINAL CORTEX LESION

It is commonly known that target dendrites degenerate after transection of their afferent axons (Matthews et al., 1960; Deller and Frotscher, 1997). Matthews et al. (1976) later investigated this degeneration in the dentate gyrus after ECL in rats (Matthews et al., 1976). They were able to show that the degeneration of the ML took place in the superficial 73% only, while the deeper parts of the ML remained without any degeneration. Wagner et al. (1983) confirmed these findings in rats by showing an increased cytochrome oxidase activity as well as glutamate decarboxylase immunoreactivity indicating a neuronal degeneration in the OML (Wagner et al., 1983). Apart from that, in later investigations shrinkage of the OML in rats was seen regularly (Steward, 1992; Henderson et al., 1998).

In more recent investigations, however, it has become more common to use mice in neuroanatomical research. As a number of neuroanatomical differences are known between mice and rats, it is wrong to conclude that lesion-induced changes described in rats, can be applied to mice without questioning (Deller et al., 2007).

6.3.1 Shrinkage of the ML in Wildtype and CAP23tg Mice

The occurrence of shrinkage of the ML after ECL has caused some controversy in literature. While in 2003 Kadish and van Groen postulated an absence of a shrinkage of the ML after ECL in mice (Kadish and van Groen, 2003), in 2009 they found a shrinkage of the mentioned layer in aged mice (Kadish and van Groen, 2009). Meanwhile, Phinney et al. (2004) have found a similar shrinkage of the ML in mice when compared to rats.

Our findings of a shrinking ML after ECL are in line with Phinney's work (Phinney et al., 2004) (Figure 18, Figure 19, and Table 6). In WT mice the mean width of the ML shrunk from 211.48µm to 173.94µm. In CAP23tg mice the mean width of the ML shrunk from 224.31µm to 173.94µm. In our findings only CAP23tg mice showed a statistically significant shrinkage of the ML after ECL. Nevertheless, in WT mice a clear trend of

the shrinkage was detected as well. It can be safely assumed that a larger number of experimental wildtype animals would have resulted in a statistically significant result as shrinkage of wildtype dentate gyrus has been demonstrated and reproduced by a number of laboratories, including our own (e.g., Del Turco et al., 2003; Phinney et al., 2004; Vuksic et al., 2011).

6.3.2 Control of the Lesion Quality with Acetylcholinesterase Staining

Acetylcholinesterase (AChE) staining has been used to study lesion quality both in rats (Jucker et al., 1996) and in mice (Del Turco et al., 2003; Phinney et al., 2004) as after ECL a dense AChE-positive fiber band can be seen in the OML (Nadler et al., 1977a; Nadler et al., 1977b; Zimmer et al., 1986; Steward, 1992; Del Turco et al., 2003). This is mainly due to sprouting of a heterotypic fiber system (cholinergic axons) (Perederiy and Westbrook, 2013). Hence, the increase of the AChE-fiber density can be used as a histochemical marker for the extent and quality of an ECL (Nadler et al., 1977a; 1977b; Del Turco et al., 2003; Phinney et al., 2004; Vuksic et al., 2011). Even though we did not systematically analyze the AChE-stained sections, because of profound previous investigations, we acted on the assumption that in our experiments AChE-staining would have the same result. Hence, we used AChE-stained sections for quality control of the lesion.

6.4 AXONAL SPROUTING AND ITS EFFECTS

6.4.1 Homotypic, Heterotypic, Homologue, and Heterologue Sprouting

Sprouting axons can be homotypic to the lesioned entorhino-dentate pathway, if glutamatergic fibers are involved, or they can be heterotypic, if involved fibers use other neurotransmitter than glutamate (Steward, 1992; Deller and Frotscher, 1997; Perederiy and Westbrook, 2013). Furthermore, they can be homologue if they originate from the same anatomical area (e.g. contralateral EC), or they can be heterologue if the origin is located in a different anatomical region (e.g. contralateral hilus) (Deller et al., 1995a). While in rats homologue and homotypic sprouting after ECL can be observed via the crossed temporo-dentate pathway (Steward, 1976; Deller et al., 1996b), in mice a relevant crossed projection from the contralateral EC is not known

of (van Groen et al., 2002; Del Turco et al., 2003; Deller et al., 2007). However, in earlier investigations sprouting of glutamatergic, hence homotypic, calretinin-positive fibers originating from MCs of both hemispheres could be witnessed (Prang et al., 2003). It has been known that such homotypic reactive sprouting can lead to functional restoration (Reeves and Steward, 1988). While in rats this heterologue sprouting stayed within the territories of their original innervation, in mice the sprouting exceeded these boundaries (Del Turco et al., 2003). Beside this sprouting Deller et al. (1995) had already shown in rats that after ECL there is also a relevant heterotypic sprouting of GABAergic fibers within the OML originating from interneurons (Deller et al., 1995b). These interneurons are also found in abundance in mice (Jinde et al., 2012; Hsu et al., 2016).

6.4.2 Axonal Sprouting After ECL in WT Mice

We did not histologically confirm a significant sprouting of the MC axons after ECL beyond the IML-boundaries in WT mice as this has already been done by others. Del Turco et al. (2003) systematically analyzed the histological effect of an ECL on mice using immunofluorescence double-labelling for PHAL and calretinin (Del Turco et al., 2003). In this study the authors were able to show that MC axons sprout to the proximal portion of the OML, forming asymmetric synapses in the denervated region, thus contradicting the traditional view of layer-specificity of axonal sprouting, which was based on experiments in rats (Deller and Frotscher, 1997). The authors pointed out in their investigations that the border between the IML and OML is not as sharp in mice as it is in rats. Thus, the trans-laminar sprouting of commissural fibers seen in mice may be a species difference (Del Turco et al., 2003; Deller et al., 2007).

Because of the earlier histological examinations by others in the laboratory, our experiments did not focus on the histological investigation of axonal sprouting after lesion. We wanted to study the functional changes and used extracellular field recordings. This form of electrophysiological investigation is, however, not sufficiently precise to detect subtle changes at the IML/OML border of WT and transgenic mice before and after ECL.

6.4.3 Axonal Sprouting After ECL in CAP23tg Mice

The ability of translaminar sprouting of MCs in mice compared to rats can be explained by the intrinsic growth competence of each species (Del Turco et al., 2003). As growth-associated proteins are expressed depending on the age of the individual (Caroni, 1997) the translaminar sprouting was suggested to be also age-dependent with stronger sprouting during the first two weeks of life (Lynch et al., 1973; Gall and Lynch, 1980, 1981; Del Turco et al., 2003). Del Turco et al. (2001) showed in an earlier investigation a strongly enhanced axonal sprouting of MC axons in neurons of CAP23-overexpressing mice, thus further supporting the hypothesis of the intrinsic growth competence (Del Turco et al., 2001). When using these CAP23tg mice in our in-vivo experiments, we were able to confirm a statistically significant expansion of the IML in the histological measurement using calretinin-staining (data not shown; Del Turco et al., 2001). Furthermore, we saw a broader sink-signal of the IML after stimulation of the contralateral hilus in electrophysiology, hence supporting the hypothesis that the sprouting axons were collaterals of MC axons originating from the contralateral hilus. Thus, we confirmed the enhanced sprouting response as described by Del Turco et al. (2001), which made us confident that the electrophysiological changes we saw are correlated with the structural changes, i.e. enhanced sprouting, as previously described (Del Turco et al., 2001).

6.5 DENERVATION-INDUCED FUNCTIONAL CHANGES

6.5.1 Functional Changes of WT Mice

Neither the electrophysiological measurements, nor the calculated CSDs revealed any statistically significant difference in WT mice before and after ECL. On the one hand the reactive axonal sprouting is believed to be quite subtle in WT mice (Del Turco et al., 2003), on the other hand a GABAergic commissural projection with a potential of reinnervation of denervated dendrites in the OML has been known for a long time (Deller et al., 1995a). The degree of GABAergic sprouting has not been investigated in mice yet, however, there seems to be a balance between inhibition and disinhibition

in WT mice, as disinhibition of the DG would facilitate seizures (Kobayashi and Buckmaster, 2003).

6.5.2 Functional Changes of CAP23tg Mice

In our experiments the CAP23tg mice exhibited a significant expansion of the IML-sink towards the OML in electrophysiological measurements together with a significantly broader calretinin-stained IML (data not shown). Furthermore, we saw a greater excitability of the GCL using FP recordings.

Our findings of the broader IML-sink are in line with previous in-vivo results on CAP23tg mice showing an enhanced sprouting of commissural glutamatergic MC axons (Del Turco et al., 2001). This sprouting of excitatory afferents could lead to the generation of EPSPs on reinnervated dendrites in the OML, thus functionally restoring the perforant path innervation.

The enhanced sprouting of the glutamatergic MC axons may be accompanied by a not so clear situation of GABAergic sprouting in CAP23tg mice. Kobayashi and Buckmaster (2003) had assumed that the inhibitory input may play a pivotal role in the regulation of the DG excitation, as disinhibition led to seizures (Kobayashi and Buckmaster, 2003). However, our data suggest an imbalance of excitation and inhibition towards excitation. Therefore, it is likely that the degree of GABAergic sprouting is functionally less relevant than the degree of glutamatergic sprouting in CAP23tg mice.

6.5.3 Comparison of WT and CAP23tg Mice

While in WT mice we were not able to see a functional difference before and after ECL, in CAP23tg mice there were remarkable changes in the electrophysiological response.

It has been generally known that the net effect of MCs on GCs is inhibitory, despite their excitatory effect (Buzsáki and Czeh, 1981; Buzsáki and Eidelberg, 1981; Douglas et al., 1983; Bilkey and Goddard, 1987). This is due to a translamellar lateral inhibition via basket-cells (Seress and Ribak, 1984; Sloviter, 1994b). However, some studies were recently able to show an excitatory influence of MCs on GCs (Ratzliff et al., 2004;

Myers and Scharfman, 2009). Jinde et al. (2013) interpreted this as part of the pathway from CA3 to GC excitation in a disinhibited condition (Jinde et al., 2013).

Our data led to the assumption that while in WT mice there might be a subtle sprouting (Del Turco et al., 2003), the overall balance of excitation and inhibition remained functionally unchanged. In contrast, in CAP23tg mice with a much stronger sprouting response (Del Turco et al., 2001) the balance of excitation and inhibition was significantly disturbed. Hence, CAP23tg mice after ECL may show the typical response under disinhibited conditions (Jinde et al., 2013). Furthermore, the specificity of the sprouting may be impaired in CAP23tg mice. Whereas commissural/associational MC axons terminate on inhibitory basket cells as well as GCs in the wildtype animal, they may preferentially reinnervate granule cells under denervation conditions. Presently, we do not have any data on this and quantitative electron microscopy will be needed to understand whether or not the target-cell specificity of the sprouting response is altered.

6.5.4 Restoration of Functionality

One may suggest that the hyperexcitation of the GCL after MC activation in lesioned CAP23tg mice could restore the actual functionality of the GCs. Indeed, the response of the GCL after MC activation in the above-mentioned mice bore some morphological similarities to the actual GCL-response after PP activation as known before (Jedlicka et al., 2009). Yet, an actual restoration of the GCL, as a component of the overall hippocampal network, through enhanced axonal sprouting of MC axons remains questionable. The network is highly unbalanced and prone to seizures due to disinhibition (Kobayashi and Buckmaster, 2003). How severe the imbalance actually is and to which degree this sensitive balance of excitation and inhibition can be restored, remains to be investigated further in future research.

7 CLINICAL IMPLICATIONS AND CONCLUSION

Axonal sprouting can be enhanced if the growth competence of sprouting neurons is modified. In CAP23tg mice the chicken-homologue (CAP23) of the intrinsic growth-associated protein NAP22 is overexpressed (Caroni et al, 1997; Voelcker, 2012), thus leading to an enhanced axonal sprouting response of MC axons after ECL (Del Turco et al., 2001). The functional relevance of this enhanced sprouting, however, has not yet been investigated so far. So the question remains, whether this kind of sprouting compared to other modalities, is beneficial for the whole organism.

If you take sprouting of homologous fibers, like the crossed temporo-dentate pathway in rats, a functional recovery can be observed (Steward, 1976; Reeves and Steward, 1988). However, in our experiments the sprouting of heterologous fibers originating from the hilar MCs was enhanced, which may not lead to complete functional recovery as the GCL seemed to become hyperexcitable. Nevertheless, this observation needs further testing in the future, especially considering the fact that this sprouting may have a relevant influence on the balance of excitation and inhibition, which we did not investigate any further.

Our data and these considerations have important therapeutic implications. It may not be functionally restorative to upregulate/increase the growth of all sprouting and reinnervating neuronal populations. Rather, therapeutic interventions should focus on increasing sprouting of the homologous and homotopic projection systems. This may be feasible, since many neurodegenerative diseases, such as Alzheimer´s disease and Parkinson´s disease, where compensatory sprouting of surviving fibers is seen, show a gradual decline of neuronal populations. Some neurons die while others are still present. If collateral sprouting of the surviving neuron populations can be enhanced, for example using gene-therapy with adeno-associated viruses, this could prove to be beneficial for patients suffering from these diseases. Thus, our data may provide an important new perspective for therapies aiming at enhancing the sprouting response following brain injury: Sprouting should be selectively enhanced in some but not in all sprouting neuron populations.

8 REFERENCES

Aigner L, Arber S, Kapfhammer J, Laux T, Schneider C, Botteri F, Brenner H, Caroni P (1995) Overexpression of the neural growth-associated protein GAP-43 induces nerve sprouting in the adult nervous system of transgenic mice. Cell 83:269-78.

Amaral DG, Witter MP (1989) The three-dimensional organization of the hippocampal formation: a review of anatomical data. Neuroscience 31(3):571-91

Andersen P, Blackstad T, Lömo T (1966) Location and identification of excitatory synapses on hippocampal pyramidal cells. Exp Brain Res. 1:236-48.

Andersen P, Bliss T, Skrede K (1971) Lamellar organization of hippocampal pathways. Exp Brain Res. 13:222–238.

Andersen P, Morris R, Amaral D, Bliss T, O'Keefe J (2007) The Hippocampus Book: Oxford University Press.

Arantius J (1587) De Humano Foetu, 1587.

Ben-Ari Y (1985) Limbic seizure and brain damage produced by kainic acid: mechanisms and relevance to human temporal lobe epilepsy. Neuroscience 14:375-403.

Bennett M, Gibson W, Robinson J (1994) Dynamics of the CA3 pyramidal neuron autoassociative memory network in the hippocampus. Philos Trans R Soc Lond B Biol Sci 343:167-87.

Benowitz L, Apostolides P, Perrone-Bizzozero N, Finklestein S, Zwiers H (1988) Anatomical distribution of the growth-associated protein GAP-43/B-50 in the adult rat brain. J Neurosci. 8:339-52.

Benowitz LI, Routtenberg A (1997) GAP-43: an intrinsic determinant of neuronal development and plasticity. Trends Neurosci 20:84–91.

Bilkey D, Goddard G (1987) Septohippocampal and commissural pathways antagonistically control inhibitory interneurons in the dentate gyrus. Brain Res. 405:320-5.

Blackstad T (1956) Commissural connections of the hippocampal region in the rat, with special reference to their mode of termination. J Comp Neurol 105:417-537.

Blackstad T (1958) On the termination of some afferents to the hippocampus and fascia dentata; an experimental study in the rat. Acta Anat (Basel) 35:202-14.

Bomze H, Bulsara K, Iskandar B, Caroni P, Skene J (2001) Spinal axon regeneration evoked by replacing two growth cone proteins in adult neurons. Nat Neurosci 4:38-43.

Bovolenta P, Wandosell F, Nieto-Sampedro M (1991) Neurite outgrowth over resting and reactive astrocytes. Restor Neurol Neurosci 2:221-8.

Brun A, Liu X, Erikson C (1995) Synapse loss and gliosis in the molecular layer of the cerebral cortex in Alzheimer's disease and in frontal lobe degeneration. Neurodegeneration 4:171-7.

Buzsáki G, Czeh G (1981) Commissural and perforant path interactions in the rat hippocampus. Field potentials and unitary activity. Exp Brain Res. 43:429-38.

Buzsáki G, Eidelberg E (1981) Commissural projection to the dentate gyrus of the rat: evidence for feed-forward inhibition. Brain Res 230:346-50.

Buzsáki G, Eidelberg E (1982) Convergence of associational and commissural pathways on CA1 pyramidal cells of the rat hippocampus. Brain Res. 237:283-95.

Caroni P (1997) Intrinsic neuronal determinants that promote axonal sprouting and elongation. Bioessays 19:767-75.

Caroni P, Aigner L, Schneider C (1997) Intrinsic neuronal determinants locally regulate extrasynaptic and synaptic growth at the adult neuromuscular junction. J Cell Biol. 136:679-92.

Ceranik K, Bender R, Geiger J, Monyer H, Jonas P, Frotscher M, Lübke J (1997) A novel type of GABAergic interneuron connecting the input and the output regions of the hippocampus. J Neurosci. 17:5380–5394.

Claiborne B, Amaral D, Cowan W (1986) A light and electron microscopic analysis of the mossy fibers of the rat dentate gyrus. J Comp Neurol. 246:435-58.

Claiborne B, Amaral D, Cowan W (1990) Quantitative, three-dimensional analysis of granule cell dendrites in the rat dentate gyrus. J Comp Neurol. 302:206-19.

Clusmann H, Nitsch R, Heinemann U (1994) Long lasting functional alterations in the rat dentate gyrus following entorhinal cortex lesion: a current source density analysis. Neuroscience 61:805-15.

Del Turco D, Gebhardt C, Woods A, Kapfhammer J, Naumann T, Frotscher M, Caroni P, Deller T (2001) Overexpression of the growth associated protein CAP23

results in translaminar commissural sprouting in the hippocampus after entorhinal cortex lesion in adult mice. Soc Neurosci Abs:27:698.12.

Del Turco D, Woods A, Gebhardt C, Phinney A, Jucker M, Frotscher M, Deller T (2003) Comparison of commissural sprouting in the mouse and rat fascia dentata after entorhinal cortex lesion. Hippocampus 13:685-99.

Deller T (1998) The anatomical organization of the rat fascia dentata: new aspects of laminar organization as revealed by anterograde tracing with Phaseolus vulgaris-Luecoagglutinin (PHAL). Anat Embryol (Berl). 197:89-103.

Deller T, Adelmann G, Nitsch R, Frotscher M (1996a) The alvear pathway of the rat hippocampus. Cell Tissue Res. 286:293-303.

Deller T, Del Turco D, Rappert A, Bechmann I (2007) Structural reorganization of the dentate gyrus following entorhinal denervation: species differences between rat and mouse. Prog Brain Res. 163:501-28.

Deller T, Drakew A, Frotscher M (1999) Different primary target cells are important for fiber lamination in the fascia dentata: a lesson from reeler mutant mice. Exp Neurol. 156:239-53.

Deller T, Frotscher M (1997) Lesion-induced plasticity of central neurons: sprouting of single fibres in the rat hippocampus after unilateral entorhinal cortex lesion. Prog Neurobiol. 53:687-727.

Deller T, Frotscher M, Nitsch R (1995a) Morphological evidence for the sprouting of inhibitory commissural fibers in response to the lesion of the excitatory entorhinal input to the rat dentate gyrus. J Neurosci. 15:6868-78.

Deller T, Frotscher M, Nitsch R (1996b) Sprouting of crossed entorhinodentate fibers after a unilateral entorhinal lesion: anterograde tracing of fiber reorganization with Phaseolus vulgaris-leucoagglutinin (PHAL). J Comp Neurol. 365:42-55.

Deller T, Nitsch R, Frotscher M (1995b) Phaseolus vulgaris-leucoagglutinin tracing of commissural fibers to the rat dentate gyrus: evidence for a previously unknown commissural projection to the outer molecular layer. J Comp Neurol. 352:55-68.

Denny J (2006) Molecular mechanisms, biological actions, and neuropharmacology of the growth-associated protein GAP-43. Curr Neuropharmacol. 4:293-304.

Desmond N, Levy W (1982) A quantitative anatomical study of the granule cell dendritic fields of the rat dentate gyrus using a novel probabilistic method. J Comp Neurol. 212:131-45.

Desmond N, Levy W (1985) Granule cell dendritic spine density in the rat hippocampus varies with spine shape and location. Neurosci Lett. 54:219-24.

Douglas R, McNaughton B, Goddard G (1983) Commissural inhibition and facilitation of granule cell discharge in fascia dentata. J Comp Neurol. 219:285-94.

Finsen B, Tønder N, Xavier G, Sørensen J, Zimmer J (1993) Induction of microglial immunomolecules by anterogradely degenerating mossy fibres in the rat hippocampal formation. J Chem Neuroanat 6:267–275.

Franklin, Paxinos (1997) Mouse Brain Atlas.

Freeman J, Nicholson C (1975) Experimental optimization of current source-density technique for anuran cerebellum. J Neurophysiol. 38:369-82.

Frey D, Laux T, Xu L, Schneider C, Caroni P (2000) Shared and unique roles of CAP23 and GAP43 in actin regulation, neurite outgrowth, and anatomical plasticity. J Cell Biol. 149:1443-54.

Gall C, Lynch G (1980) The regulation of fiber growth and synaptogenesis in the developing hippocampus. Curr Top Dev Biol 15 Pt 1:159–180.

Gall C, Lynch G (1981) Fiber architecture of the dentate gyrus following ablation of the entorhinal cortex in rats of different ages: evidence for two forms of axon sprouting in the immature brain. Neuroscience 6:903–910.

Gall C, McWilliams R, Lynch G (1980) Accelerated rates of synaptogenesis by "sprouting" afferents in the immature hippocampal formation. J Comp Neurol 193:1047–1061.

Golarai G, Sutula T (1996) Bilateral organization of parallel and serial pathways in the dentate gyrus demonstrated by current-source density analysis in the rat. J Neurophysiol. 75:329-42.

Goldman D (1943) Potential, Impedance, and Rectification in Membranes. J Gen Physiol. 27:37-60.

Goldowitz D, White W, Steward O, Lynch G, Cotman C (1975) Anatomical evidence for a projection from the entorhinal cortex to the contralateral dentate gyrus of the rat. Exp Neurol. 47:433-41.

Golgi C, Bentivoglio M, Swanson L (2001) On the fine structure of the pes Hippocampi major (with plates XIII-XXIII). 1886. Brain Res Bull 54:461–483.

Gorgels T, Van Lookeren Campagne M, Oestreicher A, Gribnau A, Gispen W (1989) B-50/GAP43 is localized at the cytoplasmic side of the plasma membrane in developing and adult rat pyramidal tract. J Neurosci. 9:3861-9.

Gray E (1959) Electron microscopy of synaptic contacts on dendrite spines of the cerebral cortex. Nature 183:1592-3.

Henderson Z, Harrison PS, Jagger E, Beeby JH (1998) Density of choline acetyltransferase-immunoreactive terminals in the rat dentate gyrus after entorhinal cortex lesions: a quantitative light microscope study. Exp Neurol. 152:50–63.

Hjorth-Simonsen A (1973) Some intrinsic connections of the hippocampus in the rat: an experimental analysis. J Comp Neurol. 147:145-61.

Hjorth-Simonsen A, Jeune B (1972) Origin and termination of the hippocampal perforant path in the rat studied by silver impregnation. J Comp Neurol. 144:215-32.

Hodgkin A, Huxley A (1952) A quantitative description of membrane current and its application to conduction and excitation in nerve. J Physiol. 117:500-44.

Holsheimer J (1987) Electrical conductivity of the hippocampal CA1 layers and application to current-source-density analysis. Exp Brain Res. 67:402-10.

Hsu T, Lee C, Tai M, Lien C (2016) Differential Recruitment of Dentate Gyrus Interneuron Types by Commissural Versus Perforant Pathways. Cereb Cortex 26:2715–2727.

Iino S, Kobayashi S, Maekawa S (1999) Immunohistochemical localization of a novel acidic calmodulin-binding protein, NAP-22, in the rat brain. Neuroscience 91:1435-44.

Jackson M, Scharfman H (1996) Positive feedback from hilar mossy cells to granule cells in the dentate gyrus revealed by voltage-sensitive dye and microelectrode recording. J Neurophysiol. 76:601-16.

Jedlicka P, Hoon M, Papadopoulos T, Vlachos A, Winkels R, Poulopoulos A, Betz H, Deller T, Brose N, Varoqueaux F, Schwarzacher S (2011) Increased dentate gyrus excitability in neuroligin-2-deficient mice in vivo. Cereb Cortex 21:357-67.

Jedlicka P, Schwarzacher S, Winkels R, Kienzler F, Frotscher M, Bramham C, Schultz C, Bas Orth C, Deller T (2009) Impairment of in vivo theta-burst long-term potentiation and network excitability in the dentate gyrus of synaptopodin-deficient mice lacking the spine apparatus and the cisternal organelle. Hippocampus 19:130-40.

Jinde S, Zsiros V, Jiang Z, Nakao K, Pickel J, Kohno K, Belforte JE, Nakazawa K (2012) Hilar mossy cell degeneration causes transient dentate granule cell hyperexcitability and impaired pattern separation. Neuron 76:1189–1200.

Jinde S, Zsiros V, Nakazawa K (2013) Hilar mossy cell circuitry controlling dentate granule cell excitability. Front Neural Circuits 7:14.

Jucker M, D'Amato F, Mondadori C, Mohajeri H, Magyar J, Bartsch U, Schachner M (1996) Expression of the neural adhesion molecule L1 in the deafferented dentate gyrus. Neuroscience 75:703–715.

Kadish I, van Groen T (2002) Low levels of estrogen significantly diminish axonal sprouting after entorhinal cortex lesions in the mouse. J Neurosci 22:4095–4102.

Kadish I, van Groen T (2003) Differences in lesion-induced hippocampal plasticity between mice and rats. Neuroscience 116:499–509.

Kadish I, van Groen T (2009) Lesion-induced hippocampal plasticity in transgenic Alzheimer's disease mouse models: influences of age, genotype, and estrogen. J Alzheimers Dis. 18:429–445.

Kaibara T, Leung L (1993) Basal versus apical dendritic long-term potentiation of commissural afferents to hippocampal CA1: a current-source density study. J Neurosci. 13:2391-404.

Kempermann G, Brandon E, Gage F (1998) Environmental stimulation of 129/SvJ mice causes increased cell proliferation and neurogenesis in the adult dentate gyrus. Curr Biol. 8:939-42.

Kempermann G, Kuhn H, Gage F (1997) More hippocampal neurons in adult mice living in an enriched environment. Nature 386:493-5.

Kleschevnikov A, Routtenberg A (2003) Long-term potentiation recruits a trisynaptic excitatory associative network within the mouse dentate gyrus. Eur J Neurosci 17:2690-702.

Knowles W (1992) Normal anatomy and neurophysiology of the hippocampal formation. J Clin Neurophysiol. 9:252-63.

Kobayashi M, Buckmaster P (2003) Reduced inhibition of dentate granule cells in a model of temporal lobe epilepsy. J Neurosci. 23:2440-52.

Krug M, Brödemann R, Matthies R, Rüthrich H, Wagner M (2001) Activation of the dentate gyrus by stimulation of the contralateral perforant pathway: evoked potentials and long-term potentiation after. Hippocampus 11:157-67.

Lees G (1991) Inhibition of sodium-potassium-ATPase: a potentially ubiquitous mechanism contributing to central nervous system neuropathology. Brain Res Brain Res Rev. 16:283-300.

Leung L, Roth L, Canning K (1995) Entorhinal inputs to hippocampal CA1 and dentate gyrus in the rat: a current-source-density study. J Neurophysiol. 73:2392-403.

Leung M, Boer H, van Minnen J, Lundy J, Stefano G (1990) Evidence for an enkephalinergic system in the nervous system of the pond snail, Lymnaea stagnalis. Brain Res. 531:66-71.

Liu P, Bilkey D (1997) Current source density analysis of the potential evoked in hippocampus by perirhinal cortex stimulation. Hippocampus 7:389-96.

Lorente de Nó R (1947) A study of nerve physiology. Stud Rockefeller Inst Med Res Repr. 132:1-548.

Lynch G, Matthews D, Mosko S, Parks T, Cotman C (1972) Induced acetylcholinesterase-rich layer in rat dentate gyrus following entorhinal lesions. Brain Res. 42:311–318.

Lynch G, Stanfield B, Cotman C (1973) Developmental differences in post-lesion axonal growth in the hippocampus. Brain Res. 59:155–168.

Maekawa S, Maekawa M, Hattori S, Nakamura S (1993) Purification and molecular cloning of a novel acidic calmodulin binding protein from rat brain. J Biol Chem. 268:13703-9.

Maier D, Mani S, Donovan S, Soppet D, Tessarollo L, McCasland J, Meiri K (1999) Disrupted cortical map and absence of cortical barrels in growth-associated protein (GAP)-43 knockout mice. Proc Natl Acad Sci U S A 96:9397-402.

Masukar AV, Srinivas KV, Brann DH, Warren R, Lowes DC, Siegelbaum SA (2017) Medial and lateral entorhinal cortex differentially excite deep versus superficial CA1 pyramidal neurons. Cell Rep. 18(1):148-160

Matsubara M, Nakatsu T, Kato H, Taniguchi H (2004) Crystal structure of a myristoylated CAP-23/NAP-22 N-terminal domain complexed with Ca2+/calmodulin. EMBO J. 23:712-8.

Matthews D, Cotman C, Lynch G (1976) An electron microscopic study of lesion-induced synaptogenesis in the dentate gyrus of the adult rat. I. Magnitude and time course of degeneration. Brain Res. 115:1–21.

Matthews M, Cowan W, Powell T (1960) Transneuronal cell degeneration in the lateral geniculate nucleus of the macaque monkey. J Anat. 94:145-69.

Megias M, Emri Z, Freund T, Gulyas A (2001) Total number and distribution of inhibitory and excitatory synapses on hippocampal CA1 pyramidal cells. Neuroscience 102:527-40.

Meiri KF, Pfenninger K, Willard M (1986) Growth-associated protein, GAP-43, a polypeptide that is induced when neurons extend axons, is a component of growth cones and corresponds to pp46, a major polypeptide of a subcellular fraction enriched in growth cones. Proc Natl Acad Sci U S A 83:3537–3541.

Morita S, Miyata S (2013) Synaptic localization of growth-associated protein 43 in cultured hippocampal neurons during synaptogenesis. Cell Biochem Funct. 31:400-11.

Myers C, Scharfman H (2009) A role for hilar cells in pattern separation in the dentate gyrus: a computational approach. Hippocampus 19:321-37.

Nadler J, Cotman C, Lynch G (1974) Biochemical plasticity of short-axon interneurons: increased glutamate decarboxylase activity in the denervated area of rat dentate gyrus following entorhinal lesion. Exp Neurol. 45:403–413.

Nadler J, Cotman C, Lynch G (1977a) Histochemical evidence of altered development of cholinergic fibers in the rat dentate gyrus following lesions. I. Time course after complete unilateral entorhinal lesion at various ages. J Comp Neurol. 171:561–587.

Nadler J, Cotman C, Paoletti C, Lynch G (1977b) Histochemical evidence of altered development of cholinergic fibers in the rat dentate gyrus following lesions. II.

Effects of partial entorhinal and simultaneous multiple lesions. J Comp Neurol. 171:589–604.

Namgung U, Valcourt E, Routtenberg A (1995) Long-term potentiation in vivo in the intact mouse hippocampus. Brain Res. 689:85-92.

Nicholson C, Freeman J (1975) Theory of current source-density analysis and determination of conductivity tensor for anuran cerebellum. J Neurophysiol. 38:356-68.

Otmakhova N, Lisman J (2000) Dopamine, serotonin, and noradrenaline strongly inhibit the direct perforant path-CA1 synaptic input, but have little effect on the Schaffer collateral input. Ann N Y Acad Sci 911:462-4.

Papez J (1995) A proposed mechanism of emotion. 1937. J Neuropsychiatry Clin Neurosci. 7:103–112.

Pare D, Llinas R (1994) Non-lamellar propagation of entorhinal influences in the hippocampal formation: multiple electrode recordings in the isolated guinea pig brain in vitro. Hippocampus 4:403-9.

Perederiy J, Westbrook G (2013) Structural plasticity in the dentate gyrus - revisiting a classic injury model. Front Neural Circuits 7:17.

Phinney A, Calhoun M, Woods A, Deller T, Jucker M (2004) Stereological analysis of the reorganization of the dentate gyrus following entorhinal cortex lesion in mice. Eur J Neurosci 19:1731-40.

Prang P, Del Turco D, Deller T (2003) Associational sprouting in the mouse fascia dentata after entorhinal lesion in vitro. Brain Res. 978:205-12.

Raisman G (1969) Neuronal plasticity in the septal nuclei of the adult rat. Brain Res. 14:25-48.

Raisman G, Field P (1973) A quantitative investigation of the development of collateral reinnervation after partial deafferentation of the septal nuclei. Brain Res. 50:241-64.

Ramón, Cajal S (1893) Estructura del asta de Ammon y fascia dentata. Anal Soc Esp Hist Nat 22.

Rapp P, Gallagher M (1996) Preserved neuron number in the hippocampus of aged rats with spatial learning deficits. Proc Natl Acad Sci U S A 93:9926-30.

Ratzliff A, Howard A, Santhakumar V, Osapay I, Soltesz I (2004) Rapid deletion of mossy cells does not result in a hyperexcitable dentate gyrus: implications for epileptogenesis. J Neurosci 24:2259-69.

Reeves T, Steward O (1988) Changes in the firing properties of neurons in the dentate gyrus with denervation and reinnervation: implications for behavioral recovery. Exp Neurol. 102:37–49.

Repressa A, Niquet J, Pollard H, Ben-Ari Y (1995) Cell death, gliosis, and synaptic remodeling in the hippocampus of epileptic rats. J Neurobiol. 26:413-25.

Ribak C, Seress L, Peterson G, Seroogy K, Fallon J, Schmued L (1986) A GABAergic inhibitory component within the hippocampal commissural pathway. J Neurosci. 6:3492–3498.

Rolls E (1996) A theory of hippocampal function in memory. Hippocampus 6:601-20.

Schaffer (1892) Beitrag zur Histologie der Ammonshornformation. Archiv für mikroskopische Anatomie 39:611-632.

Scharfman H (2007) The CA3 "backprojection" to the dentate gyrus. Prog Brain Res. 163:627-37.

Scharfman H, Schwartzkroin P (1988) Electrophysiology of morphologically identified mossy cells of the dentate hilus recorded in guinea pig hippocampal slices. J Neurosci. 8:3812–3821.

Schwartz S, Coleman P (1981) Neurons of origin of the perforant path. Exp Neurol. 74:305-12.

Scoville W, Milner B (1957) Loss of recent memory after bilateral hippocampal lesions. J Neurol Neurosurg Psychiatry 20:11–21.

Seress L, Ribak C (1984) Direct commissural connections to the basket cells of the hippocampal dentate gyrus: anatomical evidence for feed-forward inhibition. J Neurocytol 13:215-25.

Sloviter R (1994a) On the relationship between neuropathology and pathophysiology in the epileptic hippocampus of humans and experimental animals. Hippocampus 4:250-3.

Sloviter R (1994b) The functional organization of the hippocampal dentate gyrus and its relevance to the pathogenesis of temporal lobe epilepsy. Ann Neurol. 35:640-54.

Sofroniew M, Vinters H (2010) Astrocytes: biology and pathology. Acta Neuropathol. 119:7-35.

Steward O (1976) Reinnervation of dentate gyrus by homologous afferents following entorhinal cortical lesions in adult rats. Science 194:426–428.

Steward O (1980) Trajectory of contralateral entorhinal axons which reinnervate the fascia dentata of the rat following ipsilateral entorhinal lesions. Brain Res. 183:277-89.

Steward O (1992) Lesion-induced synapse reorganization in the hippocampus of cats: sprouting of entorhinal, commissural/associational, and mossy fiber projections after unilateral entorhinal cortex lesions, with comments on the normal organization of these pathways. Hippocampus 2:247-68.

Steward O, Cotman C, Lynch G (1974) Growth of a new fiber projection in the brain of adult rats: Re-innervation of the dentate gyrus by the contralateral entorhinal cortex following ipsilateral entorhinal lesions. Exp Brain Res. 20:45-66.

Steward O, Vinsant S (1978) Collateral projections of cells in the surviving entorhinal area which reinnervate the dentate gyrus of the rat following unilateral entorhinal lesions. Brain Res. 149:216-22.

Steward O, Vinsant S, Davis L (1988) The process of reinnervation in the dentate gyrus of adult rats: an ultrastructural study of changes in presynaptic terminals as a result of sprouting. J Comp Neurol. 267:203-10.

Storm-Mathisen J, Fonnum F (1972) Localization of transmitter candidates in the hippocampal region. Prog Brain Res. 36:41-58.

Van der Zee C, Nielander H, Vos J, Lopes da Silva S, Verhaagen J, Oestreicher A, Schrama L, Schotman P, Gispen W (1989) Expression of growth-associated protein B-50 (GAP43) in dorsal root ganglia and sciatic nerve during regenerative sprouting. J Neurosci. 9:3505-12.

van Groen T, Kadish I, Wyss JM (2002) Species differences in the projections from the entorhinal cortex to the hippocampus. Brain Res Bull 57:553–556.

van Groen T, Miettinen P, Kadish I (2003) The entorhinal cortex of the mouse: organization of the projection to the hippocampal formation. Hippocampus 13:133-49.

Voelcker J (2012) Quantitative Genexpressionsanalysen der axonalen wachstumsassoziierten Proteine CAP-23/NAP-22 und GAP-43 in der Substantia nigra pars compacta der Maus.

Vuksic M, Del Turco D, Vlachos A, Schuldt G, Muller C, Schneider G, Deller T (2011) Unilateral entorhinal denervation leads to long-lasting dendritic alterations of mouse hippocampal granule cells. Exp Neurol. 230:176-85.

Wagner G, Oertel W, Wolff J (1983) Entorhinal lesions result in shrinkage of the outer molecular layer of rat dentate gyrus leading subsequently to an apparent increase of glutamate decarboxylase and cytochrome oxidase activities. Neurosci Lett. 39:255-60.

Widmer F, Caroni P (1990) Identification, localization, and primary structure of CAP-23, a particle-bound cytosolic protein of early development. J Cell Biol. 111:3035-47.

Witter M (2007) The perforant path: projections from the entorhinal cortex to the dentate gyrus. Prog Brain Res. 163:43-61.

Yang J, Han H, Cui M, Wang L, Cao J, Li L, Xu L (2006) Acute behavioural stress facilitates long-term depression in temporoammonic-CA1 pathway. Neuroreport 17:753–757.

Yeckel M, Berger T (1990) Feedforward excitation of the hippocampus by afferents from the entorhinal cortex: redefinition of the role of the trisynaptic pathway. Proc Natl Acad Sci U S A 87:5832-6.

Zimmer J, Laurberg S, Sunde N (1986) Non-cholinergic afferents determine the distribution of the cholinergic septohippocampal projection: A study of the AChE staining pattern in the rat fascia dentata and hippocampus after lesions, X-irradiation, and intracerebral grafting. Exp Brain Res. 64(1):158-68

9 CURRICULUM VITAE

Persönliche Daten

Name	Mohammad Valeed Ahmed Sethi
Geburtsdatum	02. September 1985
Geburtsort	Jeddah (Saudi-Arabien)
Staatsangehörigkeit	deutsch/pakistanisch
Konfession	Muslimisch (Ahmadiyya Muslim Jamaat KdöR)
Familienstand	verheiratet seit 18.03.2009

Schulischer Werdegang

08/1992 – 06/1993	Grund- und Hauptschule MKK Bad Orb (Grundschule)
06/1993 – 07/1994	Weinberg-Schule Langenselbold (Grundschule)
08/1994 – 07/1996	Erich-Kästner-Schule Hanau (Grundschule)
08/1996 – 07/1998	Schule am Schloßplatz Hanau (Realschule)
08/1998 – 07/2005	Hohe Landesschule Hanau (Gymnasium) mit Abitur-Abschluss (Note 1,4)

Universitäre Ausbildung und Beruf

10/2005 – 11/2011	Studium der Humanmedizin an der Johann-Wolfgang-Goethe Universität Frankfurt am Main (Fachbereich 16)
08/2007	1. Abschnitt der ärztlichen Approbationsprüfung (1. Staatsexamen) (Note 3,0)
11/2011	2. Abschnitt der ärztlichen Approbationsprüfung (2. Staatsexamen) (Note 2,0)
01/2012 – 08/2016	Assistenzarzt in der Medizinischen Hochschule Hannover, Abteilung Kinderchirurgie
Seit 09/2016	Assistenzarzt im Klinikum Region Hannover, Abteilung Allgemein-, Viszeral- und Gefäßchirurgie, Klinikum Lehrte

Sprachkenntnisse

Deutsch und Urdu	Muttersprache
Englisch	Fließend in Wort und Schrift
Latein	Das große Latinum
Spanisch und Französisch	Grundkenntnisse

_____ _____

Ort, Datum **Unterschrift**

10 DANKSAGUNG

Ich danke meinem Doktorvater, Herrn Prof. Dr. Thomas Deller für die Überlassung des Themas meiner Dissertation, für die Möglichkeit, in seinem Institut wissenschaftlich arbeiten zu dürfen und für die geduldige und sorgfältige Betreuung bei der Ausfertigung der Dissertationsschrift ganz herzlich.

Des Weiteren danke ich Herrn PD Dr. Stephan Schwarzacher, Herrn PD Dr. Peter Jedlicka und Herrn Dr. Domenico del Turco für das Einführen in wissenschaftliches Arbeiten und für die Betreuung in der Versuchsphase. Außerdem gebührt Dr. Rainer Hartmann dank für die Einweisung in die CSD-Analysen sowie der wertvollen Hilfe bei der Erstellung der entsprechenden Kurven.

Mein besonderer Dank gilt den medizinisch-technischen Assistentinnen des Institutes Ute Fertig, Heike Korff, Charlotte Nolte-Uhl, Anke Biczysko und Martina Hütten für ihre geduldige und kompetente Hilfe bei allen Laborarbeiten.

Weiterhin danke ich Frau Dr. Ekaterini Copanaki, Frau Dr. Jessica Schlaudraff sowie Herrn PD Dr. Andreas Vlachos für ihre fachliche Unterstützung, vor allem im Umgang mit den Versuchstieren, der Aufarbeitung der histologischen Präparate sowie der Bedienung der Mikroskope.

Für die Hilfe bei der Korrektur des Textes danke ich meiner Cousine Frau Hadia Khan, sowie meiner guten Freundin, Frau Nicola Opitz.

Ich danke außerdem meinen Eltern, meinen vier Schwestern und meinem guten Freund, Herrn Shehzad Khawaja für ihre Motivation, die maßgeblich zum Abschluss meiner Dissertationsschrift beigetragen hat.

Ganz besonders danke ich meiner Ehefrau die mich durch ihre Liebe und Unterstützung stets in allen Lebensbereichen antreibt, mich dabei aber nicht vergessen lässt, dass meine Karriere nicht das Zentrum meines Seins darstellt.

11 SCHRIFTLICHE ERKLÄRUNG

Ich erkläre ehrenwörtlich, dass ich die dem Fachbereich Medizin der Johann Wolfgang Goethe-Universität Frankfurt am Main zur Promotionsprüfung eingereichte Dissertation mit dem Titel

“Functional changes in the dentate gyrus of wildtype and CAP23 transgenic mice following entorhinal denervation”

in dem Institut Anatomie I Klinische Neuroanatomie unter Betreuung und Anleitung von Prof. Dr. Thomas Deller mit Unterstützung durch PD Dr. Stephan Schwarzacher ohne sonstige Hilfe selbst durchgeführt und bei der Abfassung der Arbeit keine anderen als die in der Dissertation angeführten Hilfsmittel benutzt habe. Darüber hinaus versichere ich, nicht die Hilfe einer kommerziellen Promotionsvermittlung in Anspruch genommen zu haben.

Ich habe bisher an keiner in- oder ausländischen Universität ein Gesuch um Zulassung zur Promotion eingereicht. Die vorliegende Arbeit wurde bisher nicht als Dissertation eingereicht.

_____ _____

Ort, Datum **Unterschrift**